HAL open science

Interface Properties of 2D Graphene–Polydopamine Composite Electrodes in Protic Ionic Liquid-Based Electrolytes Explored by Advanced Electrogravimetry

Adnane Bouzina, Hubert Perrot, Catherine Debiemme-Chouvy, Ozlem Sel

▶ **To cite this version:**

Adnane Bouzina, Hubert Perrot, Catherine Debiemme-Chouvy, Ozlem Sel. Interface Properties of 2D Graphene–Polydopamine Composite Electrodes in Protic Ionic Liquid-Based Electrolytes Explored by Advanced Electrogravimetry. ACS Applied Energy Materials, 2022, 5 (12), pp.14934-14944. 10.1021/acsaem.2c02404 . hal-04034272

HAL Id: hal-04034272

https://hal.science/hal-04034272v1

Submitted on 7 Nov 2023

HAL is a multi-disciplinary open access archive for the deposit and dissemination of scientific research documents, whether they are published or not. The documents may come from teaching and research institutions in France or abroad, or from public or private research centers.

L'archive ouverte pluridisciplinaire **HAL**, est destinée au dépôt et à la diffusion de documents scientifiques de niveau recherche, publiés ou non, émanant des établissements d'enseignement et de recherche français ou étrangers, des laboratoires publics ou privés.

Interface properties of 2D graphene-polydopamine composite electrodes in protic ionic liquid based electrolytes explored by advanced electrogravimetry

Adnane Bouzina,[a] Hubert Perrot,[a] Catherine Debiemme-Chouvy [a,*] and Ozlem Sel[b,c,*]

[a] Sorbonne Université, CNRS, Laboratoire Interfaces et Systèmes Electrochimiques, LISE, UMR 8235, 4 Place Jussieu, 75005 Paris, France

[b] Chimie du Solide et de l'Energie, UMR 8260, Collège de France, 11 Place Marcelin Berthelot, 75231 Paris Cedex 05, France

[c] Réseau sur le Stockage Electrochimique de l'Energie (RS2E), CNRS FR 3459, 33 Rue Saint Leu, 80039 Amiens Cedex, France

Abstract: Fundamental understanding of the processes occurring at the electrode/electrolyte interfaces is of paramount importance to enhance the performance of energy storage devices. Addressing this issue requires suitable characterization tools, due to the complex nature of such interfaces. By means of electrochemical quartz crystal microbalance (EQCM) and its advanced mode, the so-called *ac*-electrogravimetry, herein we report on the interfacial properties of 2D graphene-polydopamine (ERGO-PDA) composite electrodes in diverse electrolyte compositions including a protic ionic liquid (PIL), pyrrolidinium hydrogen sulfate $[Pyr^+][HSO_4^-]$. We have performed a comparative study in $[Pyr^+][HSO_4^-]$-water binary mixture in the absence and presence of Na_2SO_4 and compared with the interfacial behavior of ERGO-PDA in 0.5 M Na_2SO_4 (pH=2) pristine electrolyte. Our EQCM and *ac*-electrogravimetric analyses reveal that the $[Pyr^+]$ ions, due to their chaotropic nature, inhibits kosmotropic Na^+ ions and water molecules approach to the interface, suppressing the contribution of electrodragged water molecules, substantially observed in the case of pristine aqueous electrolyte. Despite the dissimilarity of the charge compensation process occurring in the presence of $[Pyr^+][HSO_4^-]$, the ERGO-PDA electrode is able to maintain similar cycling stability (99% for 10000 cycles at 1000 $mV.s^{-1}$) and specific capacitance values (325 $F.cm^{-3}$) compared with the pristine aqueous electrolyte, with the advantage of superior energy density (16.3 $mWh.cm^{-3}$ *versus* 8.7 $mWh.cm^{-3}$) due to noticeably enlarged potential window in $[Pyr^+][HSO_4^-]$-water binary mixtures.

Keywords: Reduced graphene oxide, polydopamine, ionic liquids, electrode/electrolyte interface, EQCM, *ac*-electrogravimetry

1. Introduction

Continuous demand in performance enhancement of energy storage devices (*e.g.,* batteries, supercapacitors) has been stimulating the quest of novel electrode materials, as well as new electrolytes.[1-2] For supercapacitor (SC) applications, various electrode materials (such as carbon materials,[3] transition metals and conducting polymers[4]) and different class of electrolytes (ranging from aqueous,[5] organic,[6] and redox electrolytes[7]) have been widely studied. As an alternative to the relatively classical solvents, aprotic and protic ionic liquids (AILs and PILs) have also received a colossal interest as promising green electrolytes for SCs.[8-9]

Considering the diverse research efforts for finding novel electrode and electrolyte candidates, characterization of the processes occurring at the electrode/electrolyte interface (EEI) has become more important than ever.[10-13] Indeed, the ions and solvent molecules' behavior at the EEI plays an essential role and the electrolyte composition affect the overall energy storage performance. The challenge of monitoring the complex interface processes has stimulated the use of various analytical tools in combination with electrochemical methods,[10, 14-15] providing *in situ* structural, compositional and morphological information.

Among the techniques for interface characterization, electrochemical quartz crystal microbalance (EQCM) has started to attract a great deal of attention in the energy storage domain. The different modes (EQCM-R for motional resistance or multiharmonic EQCM-D for dissipation monitoring) permitted the method not only to characterize the gravimetric changes but also to study the morphological and viscoelastic/mechanical evolution of the electrode materials in response to an electrochemical solicitation.[16-18] The EQCM based methods have significantly contributed to the investigation of a variety of phenomena, *inter alia* electro-adsorption/desorption,[16-17, 19] insertion/disinsertion of ions within electrode materials,[18] and solid–electrolyte interphase (SEI) formation/evolution[20-21] can be listed. In the context of capacitive charge storage, EQCM has successfully been employed to study the electro-adsorption/desorption of ions on the carbon surface, which can be described as follows:

On negative charged surface of carbon (Q < 0)

$$Carbon|^{-} + Cations^{+} \rightleftharpoons Carbon|^{-},^{+} Cations$$ (Potential < Potential of zero charge)

On positive charged surface of carbon (Q > 0)

$$Carbon|^{+} + Anions^{-} \rightleftharpoons Carbon|^{+},^{-} Anions$$ (Potential > Potential of zero charge)

However, in the case of a multi-ions contribution to the interface processes, characterizing the role of respective species (cation, anion or solvent molecules present in the electrolyte) becomes rather difficult.[22-24] To deconvolute the global electrogravimetric response into distinct contributions, the *ac*-electrogravimetry, a methodology which combines fast quartz crystal microbalance with electrochemical impedance spectroscopy (EIS) has been proposed as a complementary tool to interface characterization.[25-26] This advanced mode envelops the benefits of QCM and EIS in a single analytical tool, keeping in mind that it is not a basic coupling. Indeed, in addition to the classical impedance transfer function (TF), it allows a second transfer function to be obtained, the so-called electrogravimetric transfer function.[25-26] The main information that can be extracted from the *ac*-electrogavimetry includes: (i) the identification of involved species by their molar mass with clearly distinguishing between anions and cations, solvated ions and free solvent contributions, (ii) their kinetics of transfer at the EEI with their contribution in the charge balance, and (iii) the relative concentration changes of these species within the electrode material.

Due to the high relevance of the classical EQCM and *ac*-electrogravimetry for interface characterization, herein they were exploited to address the interface behavior of our previously optimized 2D graphene-polydopamine (ERGO-PDA) composite electrodes.[27] Regarding the electrolytes, we were particularly interested in protic ionic liquids (PILs) electrolytes (presence of labile hydrogens) over aprotic ionic liquids (AILs) (absence of labile hydrogens). This choice is motivated by the fact that PILs have the advantage of being inexpensive and easier to produce by a simple proton transfer between a Brønsted acid and a Brønsted base, compared to the AIL counterparts.[28-29] They are normally less viscous and can exhibit relatively higher conductivities than that of AILs,[29-30] but present still lower conductivity compared to conventional organic electrolytes (such as acetonitrile[28-29]). To further increase the ionic conductivity of the PILs, they have been used either as mixtures with organic solvents[29] and more recently as PIL-water binary mixtures.[31] However, understanding the interfacial behavior of PILs as an electrolyte component especially in binary mixtures still requires further investigation, which we address in the present study. As a promising PIL electrolyte candidate, pyrrolidinium hydrogen sulfate ($[Pyr^+][HSO_4^-]$) and its binary mixture with water has been chosen.[31-32] The interfacial charge storage behavior of ERGO and ERGO-PDA is explored in the mentioned PIL based electrolyte, in the absence and presence of Na_2SO_4 and compared with that occur in pristine 0.5 M Na_2SO_4 (pH=2). Our advanced electrogravimetric study permitted us to highlight the peculiar behavior of chaotropic $[Pyr^+]$ cations hindering the water molecules approach to the EEI and the possible

implications of this behavior in charge storage performance of the 2D graphene-polydopamine composite electrodes.

2. Experimental

2.1. Preparation of the electrodes

The ERGO and ERGO-PDA electrodes were synthesized according to the procedure reported in our previous work.[27] Briefly, about 6 µL of the GO suspension was drop-casted on the gold electrode (0.2 cm^2) of a quartz resonator (9 MHz, AWSensors, Spain). The ERGO film was obtained after the electro-reduction of the GO under the chronoamperometry mode at −1 V *vs* saturated calomel electrode (SCE) for 10 min in a solution of 0.2 M PBS (pH 7.2) containing 5 mM of DA (1 $mg \cdot mL^{-1}$). In a consecutive step, the polydopamine (PDA) was electrodeposited by chronoamperometry at 0.8 V *vs* SCE for 5 min. Typical loadings (thicknesses) of the electrodes, ERGO and ERGO-PDA are 5.3 µg (180 nm), and 6.7 µg (200 nm), respectively. The loadings were estimated by QCM measurements of the quartz resonators before and after the electrode preparation. The thickness of ERGO or ERGO-PDA films were determined by field emission gun scanning electron microscopy (FEG-SEM) observation of the sample cross section (**Figures S1a-b**). The densities of the electrodes (surface area = 0.2 cm^2) were estimated to be 1.47 $g \cdot cm^{-3}$ and 1.67 $g \cdot cm^{-3}$ for ERGO and ERGO-PDA, respectively. The presence of N (characteristic of PDA) was detected for the ERGO-PDA by energy dispersive x-ray (EDX) analysis (**Figure S1d**).

2.2. Synthesis of the selected protic ionic liquid (PIL)

Pyrrolidinium hydrogen sulfate $[Pyrr^+][HSO4^-]$ was synthesized as described by Anouti *et al.*[33] The pyrrolidine (Sigma-Aldrich, 99%) (0.4 mol) was added into a two-necked round-bottomed flask which was placed in an ice bath and equipped with a reflux condenser and a dropping funnel, the latter serving for the addition of sulfuric acid (96% in water). An equimolar quantity of the sulfuric acid (0.4 mol) was added dropwise in the pyrrolidine containing flask under vigorous stirring for 2 h. The resulting product is a yellow liquid and viscous at room temperature, ascribed as $[Pyrr^+][HSO_4^-]$ (PIL).

2.3. Morphological and compositional characterizations

The cross-section of the ERGO and ERGO-PDA films was observed under a field emission gun scanning electron microscope (FEG-SEM) (Ultra55, Zeiss) operating at 5 kV. The energy dispersive spectroscopy (EDX) analysis was performed using a JEOL 2010 microscope (JEOL

Ltd, Tokyo, Japan) to examine the composition of the ERGO and ERGO-PDA films (**Figure S1c-d**). The FEG-SEM micrographs of the cross-section and the EDX spectra of ERGO and ERGO-PDA are given in the Supporting Information file, Part I (**Figures S1a-b**).

2.4. Electrogravimetric characterizations

The electrogravimetric characterizations were performed in a standard three-electrode electrochemical configuration, by using ERGO or ERGO-PDA-loaded quartz resonator as the working electrodes, SCE as the reference electrode, and a platinum grid as the counter electrode. EQCM and *ac*-electrogravimetry measurements were carried out in three different electrolyte compositions: 0.5 M Na_2SO_4 at pH=2, PIL/water (40/60 wt%) and PIL/water (60/40 wt%) + 0.5 M Na_2SO_4, at ambient temperature.

For the classical EQCM analysis, a lab made QCM coupled with Autolab potentiostat (PGSTAT12) was used. Under the gravimetric regime, frequency changes of the microbalance (Δf) can be converted into the mass change (Δm) of the ERGO and ERGO-PDA modified QCM electrode during the cycling by applying the Sauerbrey equation:[34] $\Delta m = -k_S \times \Delta f$, where k_s is the experimental calibration constant (or sensitivity factor) (16.3×10^7 Hz·g^{-1}·cm^2).[35] To verify the gravimetric regime of the microbalance, the motional resistance (R_m) values and the resonant frequency of the quartz with and without loading in the air and in the electrolytes are measured with an Agilent network analyzer (Agilent 4294A impedance analyzer) (details are given in the Supporting Information file, Part II). The resonant frequency is obtained from the maximum of the real part of the electroacoustic admittance and the typical Butterworth-Van Dyke (BVD) equivalent circuit is used to fit this admittance to extract the values of the R_m.[36] Then, the ΔR_m values were converted into ΔW (full width at half maximum of the resonance peak) to verify that the $\Delta W \ll \Delta f$ condition is fulfilled.

For *ac*-electrogravimetry measurements,[25] a four-channel frequency response analyzer (FRA, Solartron 1254) and a lab-built potentiostat were used. The modified working electrode, on the QCM surface, was polarized at selected potentials and a sinusoidal small amplitude potential perturbation (50 mV) was applied. The frequency range of the measurements was between 63 kHz and 10 mHz. The mass change, Δm, of the working electrode was measured simultaneously with the *ac* response, ΔI, of the electrochemical system, which allowed the mass/potential transfer function (TF) ($\Delta m/\Delta E(\omega)$) to be measured along with the classical electrochemical impedance ($\Delta E/\Delta I(\omega)$) at a given potential and frequency modulation, f (pulsation, $\omega = 2\pi f$). The electrochemical TF, ($\Delta E/\Delta I(\omega)$), is presented in the form of charge/potential TF, $\Delta q/\Delta E(\omega)$,

which can decouple the charged species contributions as semi-circles, providing that their time-constants are distinct from one another. Details of the *ac*-electrogravimetry theory and data fitting procedure are given in the previous references[19, 37] and in the Supporting Information File, Part III.

3. Results and Discussion

The interface properties of the ERGO and ERGO-PDA composite electrodes were studied in $[Pyr^+][HSO_4^-]$-water binary mixture in the absence/presence of Na_2SO_4 and compared with the behavior of electrodes in the baseline electrolyte, 0.5 M Na_2SO_4. In order to have a rational correlation between different media, the aqueous 0.5M Na_2SO_4 electrolyte pH is adjusted to 2 by H_2SO_4, since the pH of $[Pyr^+][HSO_4^-]$-water binary mixture is 1.7 and 2, in the absence and presence of Na_2SO_4, respectively. The processes occurring at the interface during electrochemical cycling are studied by employing EQCM and *ac*-electrogravimetry tools.

3.1. Electrogravimetric behavior of ERGO and ERGO-PDA in 0.5M Na_2SO_4 pH 2:

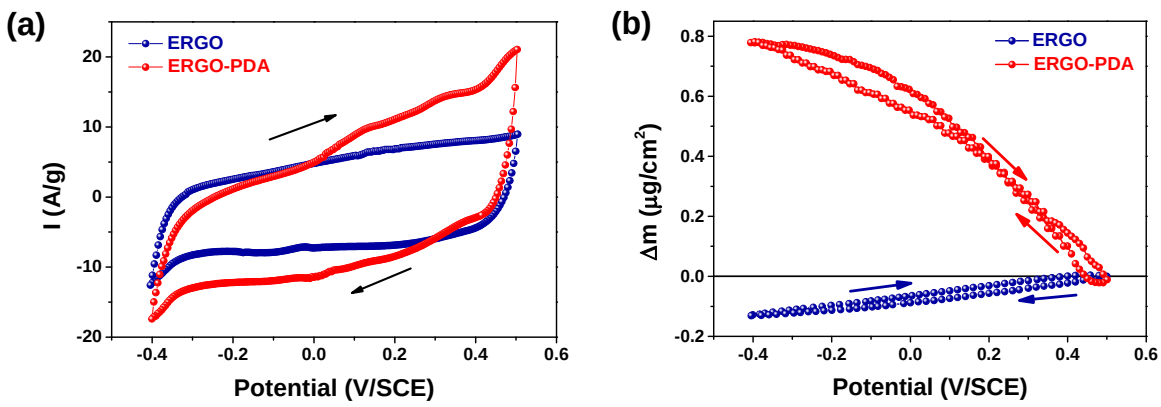

Figure 1. EQCM results in (a) CV response and (b) mass change *vs* applied potential of ERGO and ERGO-PDA at a scan rate of 50 $mV \cdot s^{-1}$ in 0.5 M Na_2SO_4 (pH=2). The current responses are normalized by the electrode loadings (panel a) whereas the Δm is normalized by the gravimetric surface area of the electrode (panel b).

The EQCM responses of the ERGO and ERGO-PDA electrodes at a scan rate of 50 $mV \cdot s^{-1}$ in Na_2SO_4 at pH = 2 are shown in **Figure 1**. CV curves show a larger integral area for ERGO-PDA compared to ERGO (**Figure 1a**), indicating a higher electroactive surface area for the charge storage process of the composite electrode, keeping in mind that the electrodes have similar loadings (5.6 μg and 6.5 μg, respectively). Simultaneous microbalance frequency

changes obtained during electrochemical cycling are converted into mass changes, justified by the electroacoustic impedance studies (**Tables S1** and **S2**). The mass of the ERGO-PDA electrode decreases and increases during the anodic and the cathodic sweep of potential, respectively (**Figure 1b**), which can indicate a major cation-exchange. While for the bare ERGO electrode, anions seem to dominate the charge compensation process, as during the anodic and the cathodic sweep, the mass increases and decreases, respectively. The inverse and ~7 times enhanced Δ*m* response of the composite electrode compared with the ERGO persists at different scan rates (**Figure S2**). To elucidate the origin of this distinct change in the electrogravimetric behavior, the *ac*-electrogavimetry was used to explore the possible contribution of multi-species, as it was observed in previous ERGO studies in other aqueous electrolytes.[19, 37-38]

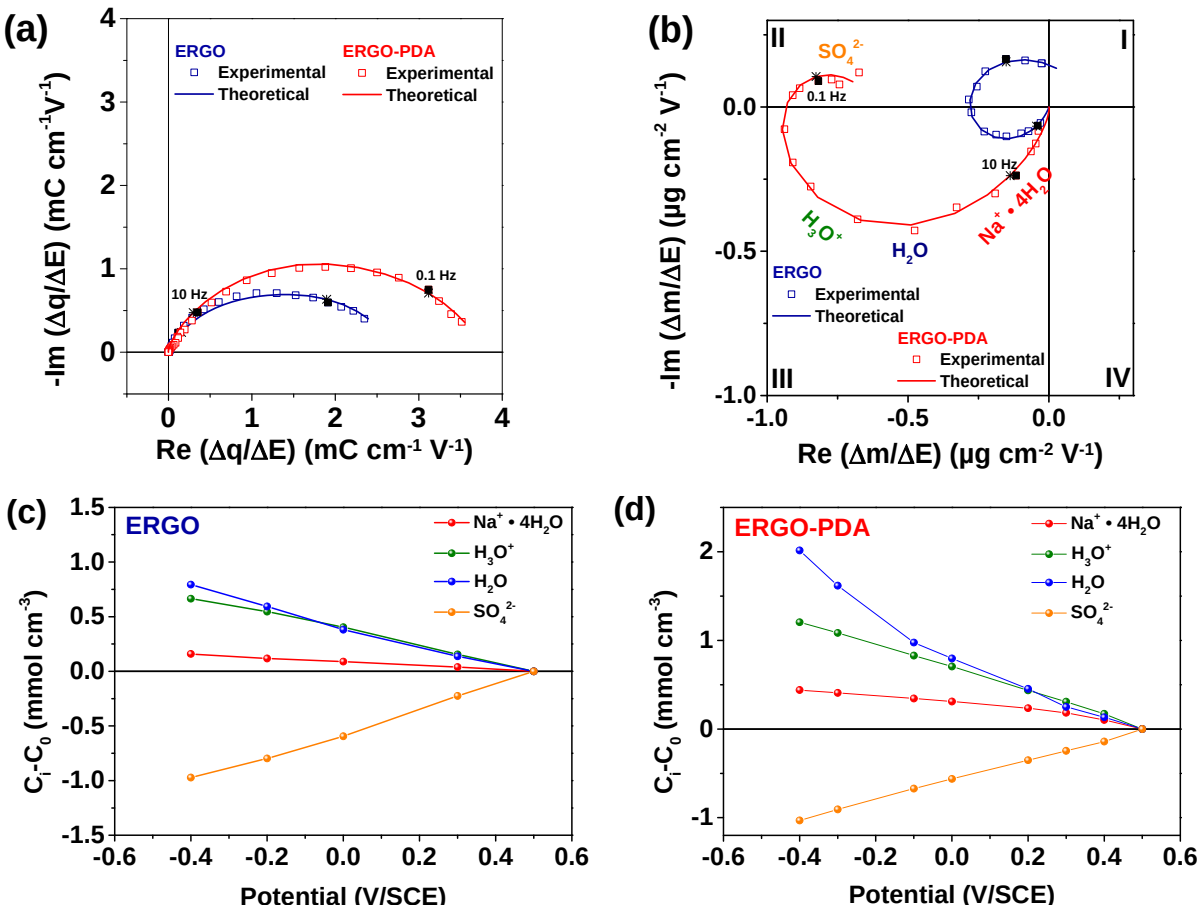

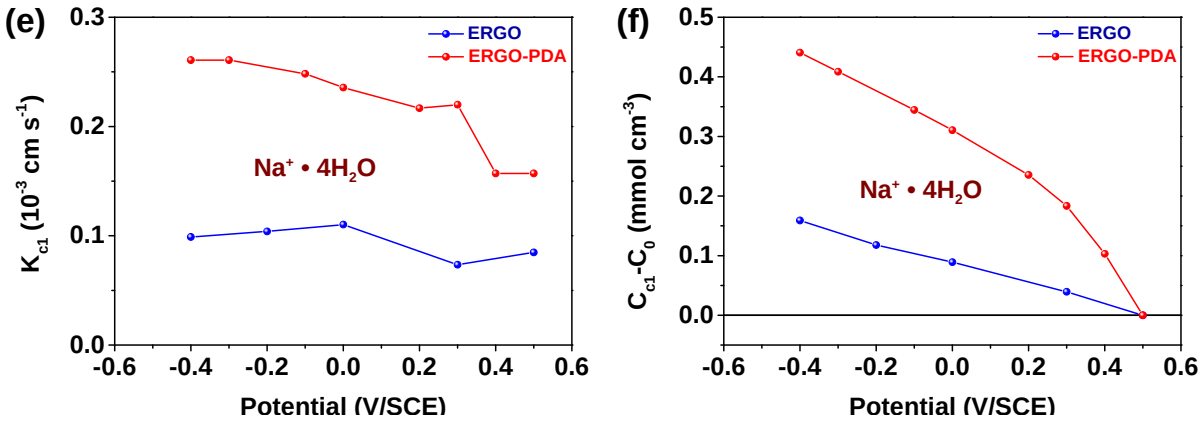

Figure 2. Experimental and theoretical *ac*-electrogravimetric data of ERGO and ERGO-PDA at 0 V *vs* SCE, (a) $\Delta q/\Delta E(\omega)$ and (b) $\Delta m/\Delta E(\omega)$ TFs. Evolution of the relative concentration change, C_i-C_0, in (c) ERGO and in (d) ERGO-PDA of the charged and non-charged species over the applied potential range, estimated from the *ac*-electrogravimetric data fitting. Kinetic constants of interfacial transfer of the hydrated cations ($Na^+ \bullet 4H_2O$) (Kc_1) (e) and its relative concentration change, C_{c1}-C_0 in ERGO and ERGO-PDA thin films (f). All the measurements are performed in 0.5 M Na_2SO_4 (pH=2).

The *ac*-electrogravimetry measurements were performed at different stationary potentials in the potential window of the CV measurements in **Figure 1**. **Figure 2a** and **2b** present the charge/potential TF, $\frac{\Delta q}{\Delta E}(\omega)$ and the electrogravimetric TF, ($\frac{\Delta m}{\Delta I}(\omega)$) at a potential of 0 V *vs* SCE where the experimental data were fitted using **Equations 1** and **2**.

$$\frac{\Delta q}{\Delta E}(\omega)\Big|_{th} = F d_f \sum_i \frac{G_i}{j\omega d_f + K_i}(\omega) \quad \text{(i: charged species)} \qquad \textbf{Equation 1}$$

$$\frac{\Delta m}{\Delta E}(\omega)\Big|_{th} = -d_f \sum_i M_i \frac{G_i}{j\omega d_f + K_i}(\omega) \quad \text{(i: (non)charged species)} \qquad \textbf{Equation 2}$$

In these equations, K_i represents the kinetics of interfacial transfer, G_i (inverse of the transfer resistance, R_{ti}) describes the ease or difficulty of interfacial transfer for each species at the electrode/electrolyte interface, where ω is the pulsation, d_f is the average film thickness, F is the Faraday constant, and M_i is the molar mass of the involved species in charge compensation process. The charge/potential transfer functions, $\frac{\Delta q}{\Delta E}(\omega)$ of both electrodes exhibit a relatively suppressed loop (**Figure 2a**), which can be related to the contribution of more than one charged species with a similar time constant. It should be noted that the loop diameter is larger for the ERGO-PDA composite film compared to the pristine ERGO, which indicates a better capacitive behavior of the composite electrode, in agreement with the increased integral area of the CV curves in **Figure 1**.

The data analysis involves testing of several configurations to fit the experimental curves. We consider several charged and non-charged species (also their hydrated counterparts) in Na_2SO_4 (pH=2) electrolyte, while keeping in mind that a good agreement between the experimental and the theoretical TFs in terms of shape and frequencies was required. **Figure 2b** depicts an example of a mass/potential TF at 0 V *vs* SCE where three charged species participate to the electroadsorption process, *i.e.,* $Na^+ \bullet 4H_2O$, H_3O^+, SO_4^{2-}, also revealing an indirect contribution of free H_2O to interfacial process. The interfacial transfer kinetics (K_i) of these four species obtained from the fitting process are presented as a function potential in **Figure S3**. Hydrated sodium species are exchanged at high frequencies, the protons, H_3O^+, participate at intermediate frequencies and SO_4^{2-} at low frequencies, corresponding to the loop located in the fourth quadrant, as seen in **Figure 2b**. The kinetic constants of the free solvent molecules are found to be close to that of $Na^+ \bullet 4H_2O$ which suggests that they are electrodragged together with hydrated Na^+.

Another important outcome of the *ac*-electrogravimetry is the relative concentration changes of the active species of, $C_i - C_0$ as a function of the potential. This quantity is estimated from the concentration potential transfer function at low frequencies as follows:

$$C_i - C_0 = \int_{E_0}^{E_1} \frac{\Delta C_i}{\Delta E}(\omega)\, dE \Big|_{\omega \to 0} = \int_{E_0}^{E_1} \frac{-G_i}{K_i}\, dE \qquad \textbf{Equation 3}$$

Then, **Figure 2c** and **2d** present C_i–C_0 of individual species identified from *ac*-electrogravimetry in the charge compensation process of ERGO and ERGO-PDA, respectively. Multi-species contribution is totally consistent with former results obtained for carbon based electrodes tested under similar conditions (in NaCl, KCl and LiCl).[19, 37] However, the repartition of each species is different depending on the electrodes' nature (**Figure 2c** and **2d**). It is noted that a significant free water contribution is observed in the potential range from -0.4 to 0.5 V *vs* SCE, with an enhancement in its quantity for the ERGO-PDA electrode (**Figure 2d**). The relative concentration increase of the hydrated sodium cation is more significant and its transfer kinetic is almost twice faster in ERGO-PDA than in ERGO (**Figure 2e** and **2f**). This is consistent with the higher *d*-spacing between the graphene sheets and the better rate capability of the ERGO-PDA electrode compared with the ERGO, that was reported in our previous work.[27]

Multi-species presence in the charge-compensation and significant amount of water contribution prompted us to change the classical electrolyte composition to $[Pyr^+][HSO_4^-]$-water binary mixture in the absence and presence of Na_2SO_4. It is noted that this binary mixtures

are of interest for enlarging the operating potential window when used as electrolytes in supercapacitor devices.

3.2. Electrogravimetric behavior of ERGO and ERGO-PDA in [Pyr^+][HSO_4^-]-water binary mixture:

PIL, pyrrolidinium hydrogen sulfate [Pyr^+][HSO_4^-] is a viscous liquid. For this reason, the optimum composition of [Pyr^+][HSO_4^-]-water binary mixture is determined based on the ionic conductivity and the viscosity. **Figure S4** shows the variation of the ionic conductivity of [Pyr^+][HSO_4^-]-water binary mixture as a function of water mass ratio (wt%) at room temperature. From this figure, it is clear that the ionic conductivity of the mixture increases progressively as the water content becomes higher. After reaching a maximum value of 184.5 $mS \cdot cm^{-1}$ for a [Pyr^+][HSO_4^-]-water weight ratio of 40/60, the ionic conductivity starts to decrease with increasing the water content, this phenomenon can be explained by the decrease of the charge carriers concentration due to dilution effect.[31] It is noted that the obtained ionic conductivity values of the [Pyr^+][HSO_4^-]-water binary mixture are in agreement with the reported values.[31-32] In addition to ionic conductivity, we also measured the motional resistance (R_m) of a bare quartz resonator by a network analyzer, to verify the optimized electrolyte composition for the EQCM studies. The R_m reveals information about acoustic energy dissipation of the quartz resonator. It can be used as an indicator of the viscoelastic properties changes of QCM resonator and its hydrodynamic interactions in contact with liquids.[18, 39-40] A drastic increase of the motional resistance of the quartz indicates significant increase of the surrounding liquid viscosity. The high R_m value of the pure ionic liquid (**Figure S4**) is explained by its high viscosity. As the water content increases, the R_m decreases due to the diminution of the viscosity of the binary electrolyte. For [Pyr^+][HSO_4^-]-water binary mixture with the highest ionic conductivity value (60 wt% of water), an R_m value of 500 Ω was obtained, this value is comparable to the values usually obtained in aqueous electrolytes with "fine-lapped quartz resonators", which ensures a gravimetric regime/stability of the QCM in this mixture. Then, the [Pyr^+][HSO_4^-]-water binary mixture of wt% of 40/60 is considered as the optimal composition for the electrogravimetric characterizations.

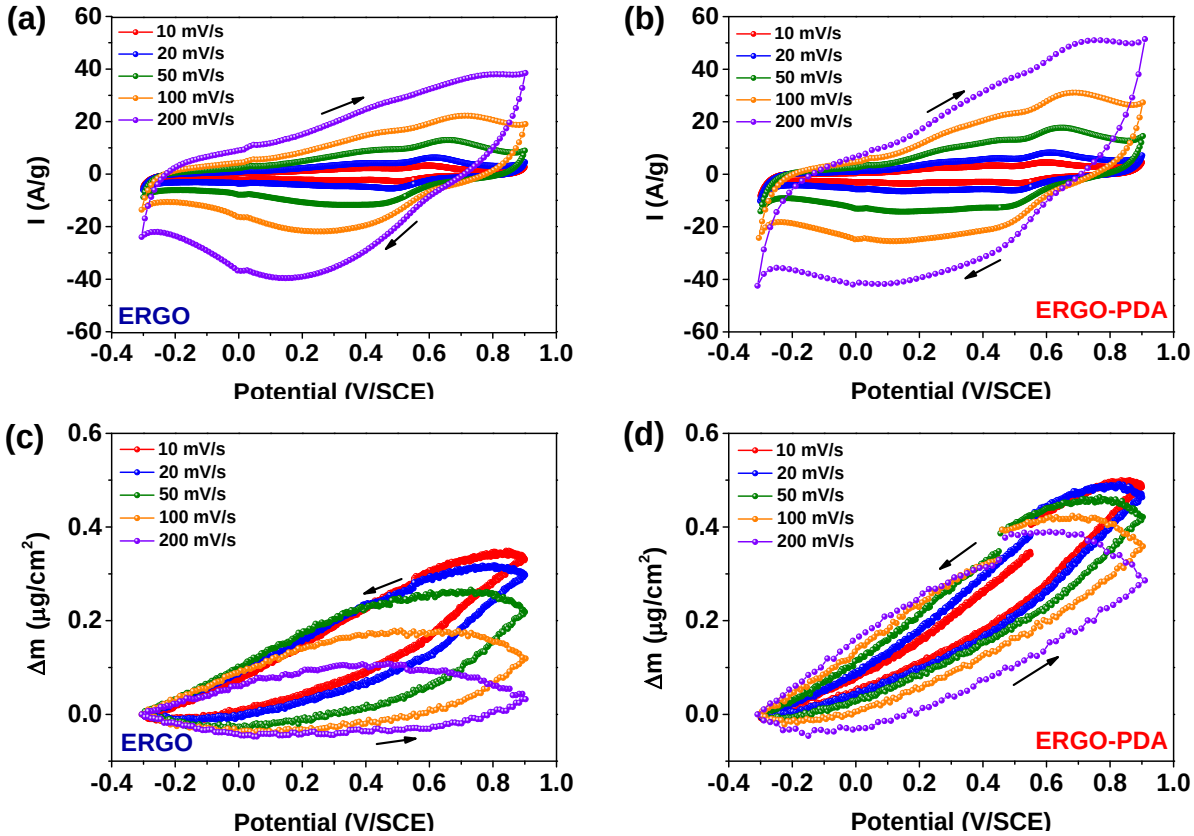

Figure 3. (a-b) CV and (c-d) mass change *vs* applied potential of ERGO and ERGO-PDA at different potential scan rates in PIL/water (40/60 wt%).

Figure 3 shows the EQCM responses of the ERGO and ERGO-PDA in the PIL/water (40/60 wt%) electrolyte. **Figure S5** shows the equivalent measurements in PIL/water + 0.5 M Na_2SO_4. In these two protic ionic liquid-based electrolytes, we can clearly see that both electrodes show a clear pseudo-capacitive contribution to the global capacitive response, as revealed by the broad reduction–oxidation peaks. Such a phenomenon was previously observed for functionalized activated carbon electrodes tested in similar protic ionic liquids,[41-44] and it was attributed to the (i) electrochemical reactions originated from the oxygenated groups of carbon surface (such as quinone/hydroquinone pairs or pyrone-like structures) which can accept two protons and two electrons and (ii) to the reversible hydrogen electrosorption. The ERGO-PDA composite shows more pronounced faradaic contributions (bumps at around 0.7 V *vs* SCE on CV, **Figure 3b** and **S5b**) than the pristine ERGO, which can be explained by the higher amount of catechol type groups for the ERGO-PDA due to the presence of the polydopamine.

Turning to the electrogravimetric behavior, based on the mass variation *vs* potential occuring during CV in PIL/water (**Figure 3c** and **3d**) and PIL/water + 0.5 M Na_2SO_4 (**Figure S5c** and **S5d**), we can say that the anions dominate the charge compensation process for both electrodes.

Contrary to the ERGO-PDA composite, the pristine ERGO's mass response shows quite significant dependence on the scan rate in PIL/water binary mixture (**Figure 3c**). Its global mass varies from 0.33 µg.cm^{-2} at 10 mV·s^{-1} to 0.036 µg.cm^{-2} at 200 mV·s^{-1} (recorded at 0.9V) which suggests a slow transfer kinetics of anionic species in this electrode (**Figure 3c**). The *ac*-electrogravimetric results in the PIL/water and PIL/water + 0.5 M Na_2SO_4 are presented in **Figure 4** (at 0 V *vs* SCE). Charge/potential TF, $\frac{\Delta q}{\Delta E}(\omega)$, presents loops with a larger diameter in the case of the ERGO-PDA composite, evidencing the positive effect of the PDA on the global capacitive response of the electrode in this complex electrolyte (**Figures 4a** and **4c**). Through the fitting of experimental TFs using theoretical TFs mentioned in **Eq.1** and **Eq.2**, only ionic species seem to participate in the charge balance. **Figures 4b** and **4d** show the electrogravimetric TF, $\frac{\Delta m}{\Delta E}(\omega)$, in the PIL/water in the absence and presence of Na_2SO_4, respectively. In both media, the ionic species are identified, demonstrating an interfacial kinetics of transfer from high to low as Pyr^+, H^+ and SO_4^{2-}, *i.e.,* Pyr^+ species appear at high frequencies, H^+ at intermediate frequencies, and SO_4^{2-} anions were detected at low frequencies.

The other possible configurations for the charge compensation process (*e.g.* HSO_4^- or H_3O^+) have been discarded due to the unsatisfactory fit of the charge/potential and mass/potential TFs (**Figure S6** and **S7**). The absence of free water molecules in the two PIL-based electrolytes and/or hydrated ions can be explained by the chaotropic behavior of Pyr^+ cations, which permits them to remain effectively dehydrated, and acts as a barrier that prevents the intervention of water molecules, either in the hydration shell or as free H_2O molecules, in the confined space between the graphene sheets. Even after adding 0.5 M Na_2SO_4 to the binary mixtrure PIL/water, Pyr^+ inhibits the highly kosmotropic Na^+ ions and water molecules approach to the interface,[45-46] suppressing the contribution of water molecules (**Figures 4d**), substantially observed in the pristine aqueous electrolyte (**Figure 2**).

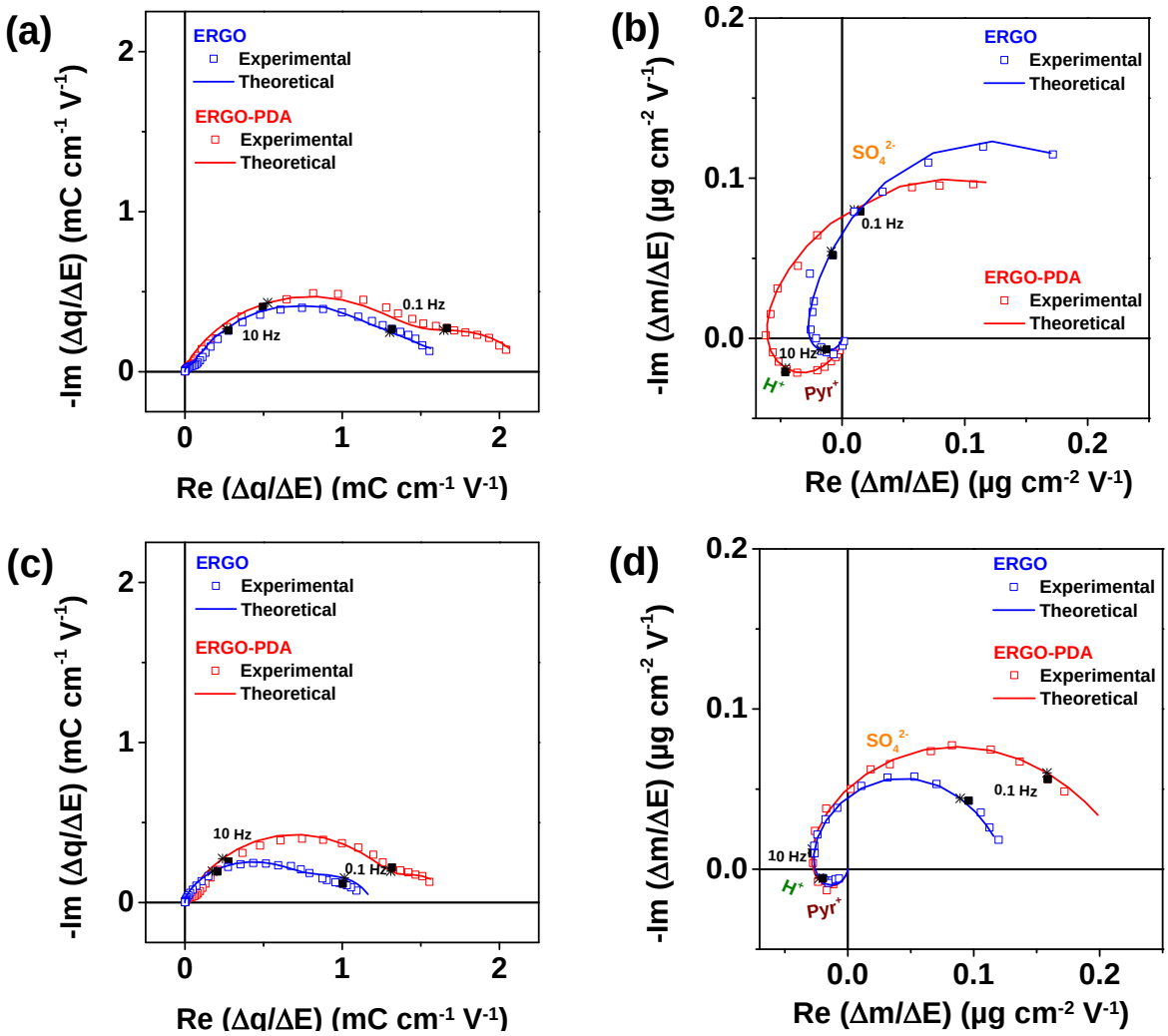

Figure 4. Experimental and theoretical *ac*-electrogravimetric data of ERGO and ERGO-PDA at 0 V *vs* SCE, (a) $\Delta q/\Delta E(\omega)$ and (b) $\Delta m/\Delta E(\omega)$ in $[Pyr^+][HSO_4^-]$-water binary mixture (60/40 wt%) and (c) $\Delta q/\Delta E(\omega)$ and (d) $\Delta m/\Delta E(\omega)$ in $[Pyr^+][HSO_4^-]$-water binary mixture (60/40 wt%) in presence of 0.5 M Na_2SO_4.

Further analyses of the K_i and G_i parameters for the three ionic species in PIL/water and PIL/water + 0.5 M Na_2SO_4 (**Tables 1** and **2**) provide insights about the dominant species in the charge compensation mechanism and the role of H^+ and SO_4^{2-}. The ratio % G_i/K_i which relates the contribution of each species in the charge balance, was also calculated using **Eq. 3** and **Eq. S6-S9**, at two different potentials (0 and 0.5V *vs* SCE). It is important to mention the major role of H^+ in the charge balance, compared to Pyr^+ and SO_4^{2-} (**Tables 1** and **2**), but its gravimetric contribution to global mass response is insignificant compared to that of the anions, SO_4^{2-},

because of low molar mass of H^+. It should be underlined that only the *ac*-electrogravimetric tool permits this kind of calculations.

The transfer kinetics of the ionic species detected in PIL/water electrolyte are higher in the ERGO-PDA composite electrode than that occurs in pristine ERGO (**Table 1** and **2**). For instance, the anions, SO_4^{2-}, are two times slower in ERGO, which can explain the observed scan rate dependency of the EQCM mass profiles of the pristine ERGO (**Figure 3c**). When 0.5 M Na_2SO_4 is present in PIL/water binary electrolyte, a significant improvement of transfer kinetics of the SO_4^{2-} was observed (**Table 2**). This is probably due to the increase of the concentration of the anions in the solution by adding 0.5 M Na_2SO_4.

Table 1. K_i (kinetics of transfer) and G_i (inverse of the transfer resistance), values obtained from the fitting of the *ac*-electrogravimetric data measured in "[Pyr^+][HSO_4^-]-water binary mixture (60/40 wt%)" at 0 and 0.5 V *vs.* SCE for ERGO and ERGO-PDA electrodes.

Electrode	**0V *vs* SCE ([Pyr^+][HSO_4^-]-water binary mixture (60/40 wt%))**								
	K_i (10^{-6} cm·s^{-1})			**G_i (10^{-8} mol·s^{-1}·cm^{-2}·V^{-1})**			**% G_i/K_i**		
	Pyr^+	**H^+**	**SO_4^{2-}**	**Pyr^+**	**H^+**	**SO_4^{2-}**	**Pyr^+**	**H^+**	**SO_4^{2-}**
ERGO	485	123	3	1	8	-0.1	3	64	33
ERGO-PDA	575	207	8	3	15	-0.3	4	64	32
	0.5V *vs* SCE ([Pyr^+][HSO_4^-]-water binary mixture (60/40 wt%))								
	K_i (10^{-6} cm·s^{-1})			**G_i (10^{-8} mol·s^{-1}·cm^{-2}·V^{-1})**			**% G_i/K_i**		
	Pyr^+	**H^+**	**SO_4^{2-}**	**Pyr^+**	**H^+**	**SO_4^{2-}**	**Pyr^+**	**H^+**	**SO_4^{2-}**
ERGO	226	72	4	0.7	6	-0.2	2	64	33
ERGO-PDA	377	134	7	3	16	-0.4	4	63	33

Table 2. K_i (kinetics of transfer) and G_i (inverse of the transfer resistance), values obtained from the fitting of the *ac*-electrogravimetric data measured in "[Pyr^+][HSO_4^-]-water binary mixture (60/40 wt%) in presence of 0.5 M Na_2SO_4" at 0 and 0.5 V *vs.* SCE for ERGO and ERGO-PDA electrodes.

Electrode	**0 V *vs* SCE ([Pyr^+][HSO_4^-]-water binary mixture (60/40 wt%) in presence of 0.5 M Na_2SO_4)**

	K_i (10^{-6} cm·s^{-1})			G_i (10^{-8} mol·s^{-1}·cm^{-2}·V^{-1})			% G_i/K_i		
	Pyr^+	**H^+**	**SO_4^{2-}**	**Pyr^+**	**H^+**	**SO_4^{2-}**	**Pyr^+**	**H^+**	**SO_4^{2-}**
ERGO	594	205	31	2	12	-0.6	4	70	26
ERGO-PDA	952	368	38	4	25	-1	4	64	32
	0.5V *vs* SCE ([Pyr^+][HSO_4^-]-water binary mixture (60/40 wt%) in presence of 0.5 M Na_2SO_4)								
	K_i (10^{-6} cm·s^{-1})			**G_i (10^{-8} mol·s^{-1}·cm^{-2}·V^{-1})**			**% G_i/K_i**		
	Pyr^+	**H^+**	**SO_4^{2-}**	**Pyr^+**	**H^+**	**SO_4^{2-}**	**Pyr^+**	**H^+**	**SO_4^{2-}**
ERGO	197	112	20	1	9	-0.5	5	70	25
ERGO-PDA	408	196	31	4	19	-1	6	68	26

3.3. Correlation of the classical EQCM and *ac*-electrogravimetric analyses:

In order to validate our hypothesis implying a multi-species contribution in the charge balance, a methodology taking advantage of the complementarity between the EQCM and *ac*-electrogravimetry is used. The applied approach uses the charge fractions and the flux direction of each species estimated from *ac*-electrogravimetry to obtain a total $\Delta m_{ac\text{-}QCM}$ (**Figure 5**). **Equations S6-S9** permitted the charge fractions to be estimated using the $-G_i/K_i$ values, which characterizes the concentration variation of each species due to a potential variation ($\Delta C/\Delta E(\omega)$) (**Equation 3**) (**Table 1, 2, S3** and **S4**). Then, these charge fractions are injected into **Equation S10** and **S11**. The global mass taking into account the presence of the different species was calculated using **Equation S10** (the charge ($Q-Q_0$) corresponds to anodic sweep of potential of the CV responses at 10 mV·s^{-1}). From **Figure 5**, one can clearly see that the reconstructed masses for the *ac*-electrogravimetry and the mass changes measured in EQCM present a satisfactory agreement in the aqueous electrolyte (0.5 M Na_2SO_4), as well as in PIL/water and PIL/water + 0.5M Na_2SO_4 solutions. This verification step confirms the multispecies participation in charge-storage for both electrodes (ERGO and ERGO-PDA) in the three different electrolytes studied. Indeed, the global mass variations obtained by classical EQCM

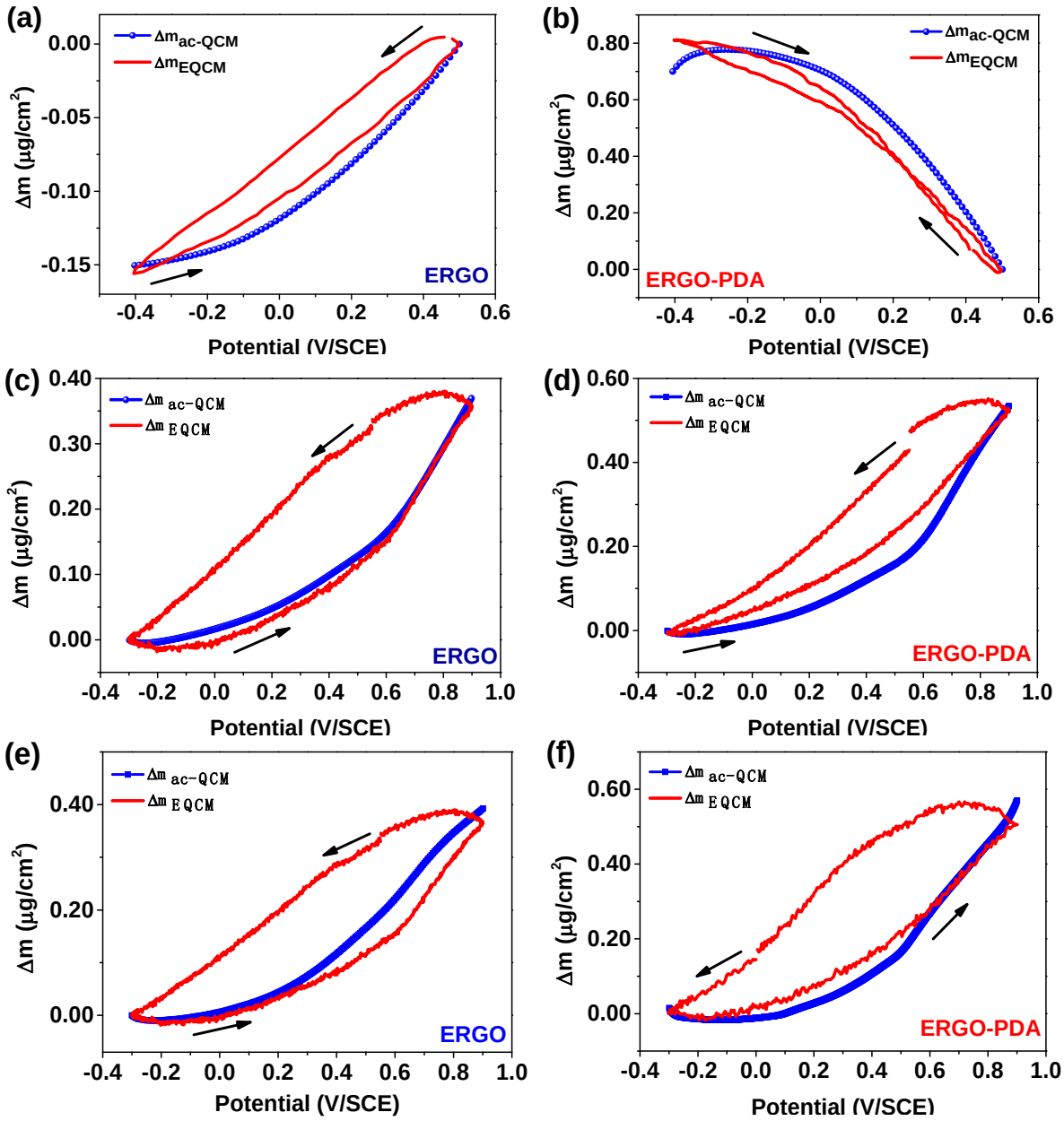

Figure 5. Comparisons of total mass variation estimated from *ac*-electrogravimetry ($\Delta m_{ac\text{-}QCM}$) and from classical EQCM (Δm_{EQCM}) for ERGO and ERGO-PDA electrodes in (a, b) 0.5 M Na_2SO_4 (pH=2), (c,d) PIL/water (60/40 wt%) and (e, f) PIL/water (60/40 wt%) + 0.5 M Na_2SO_4.

at low scan rates (in **Figures S2c-d, 3c-d** and **S5c-d**) are the cumulative response of multi-species as deconvoluted by *ac*-electrogravimetry (in **Figures S8c-d, S9a-b** and **S10a-b**). This study demonstrates the sensitivity of the *ac*-electrogravimetry to unveil the interfacial processes in the presence of diverse charge carriers and even in complex electrolyte compositions. Through incorporation of Na_2SO_4 in PIL/water binary mixtures, we could clearly highlight the impact of the cations' nature on the interface behavior. Although Pyr^+ cations' contribution to

charge compensation is minor (~5% in **Table 1-2**) compared to H^+ and SO_4^{2-}, it has a significant impact in hindering the participation of Na^+ species and water molecules (either in the solvation shell or as free H_2O molecules) into the charge compensation process.

In the next section, the electrochemical charge storage of ERGO-PDA composite is tested in PIL/water and PIL/water + 0.5M Na_2SO_4 solutions to investigate any possible consequence of such a hindrance on performance and will be compared to that in aqueous 0.5M Na_2SO_4 pH=2 electrolyte.

3.4. Electrochemical charge storage performance of ERGO-PDA electrode:

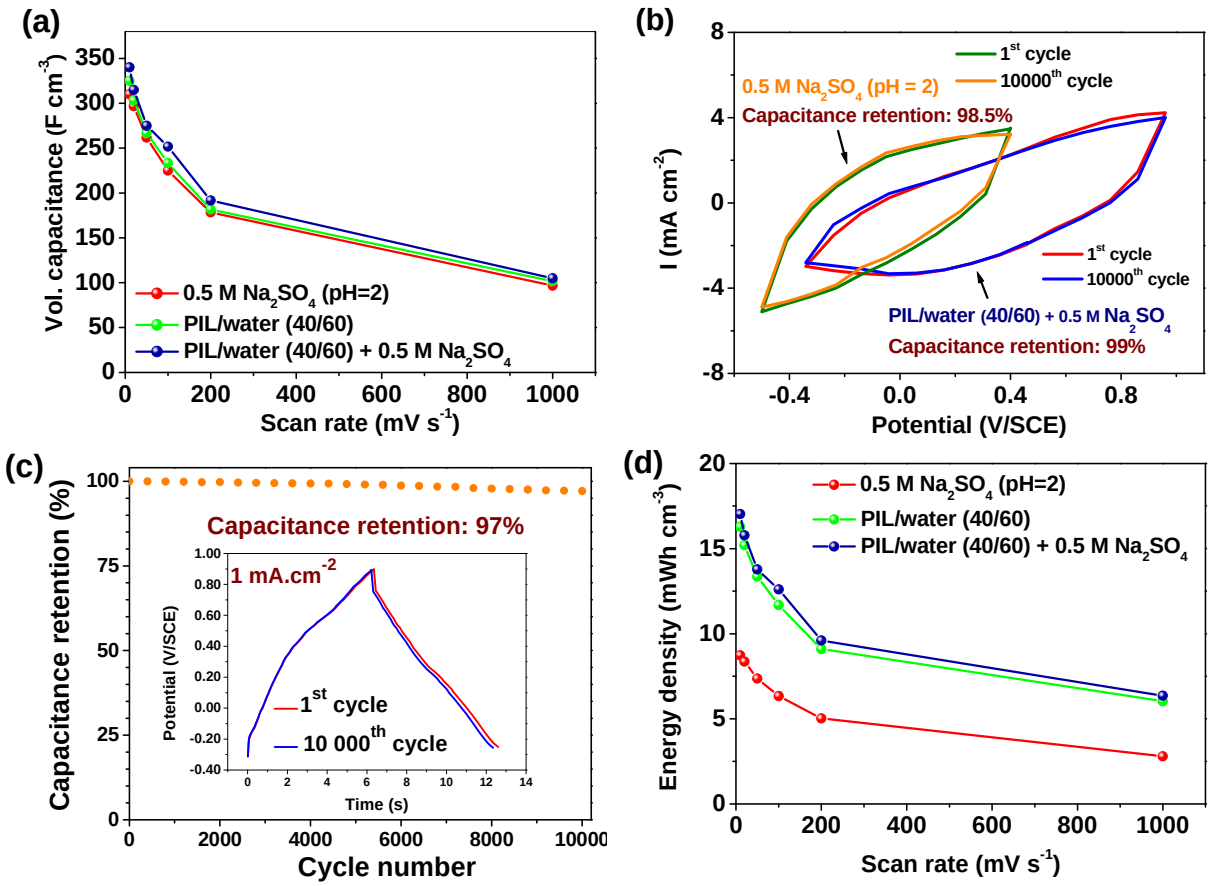

Figure 6. (a) Volumetric capacitance *vs*. potential scan rate in 0.5 M Na_2SO_4 (pH=2), PIL/water (60/40) and PIL/water (60/40 wt%) + 0.5 M Na_2SO_4, (b) capacitance retention of ERGO-PDA in 0.5 M Na_2SO_4 (pH=2) and PIL/water (60/40 wt%) + 0.5 M Na_2SO_4 at a scan rate of 1 $V \cdot s^{-1}$, (c) capacitance retention of ERGO-PDA in PIL/water (60/40 wt%) + 0.5 M Na_2SO_4 at a current density of 1 $mA \cdot cm^{-2}$ and (d) the energy density of ERGO-PDA as a function of the scan rate, compared in three different electrolytes.

The volumetric capacitance and energy density of the composite ERGO-PDA as a function of the scan rate are calculated using **Equations 4-6**, and the corresponding results are displayed in **Figure 6**.

$$C_S(F.g^{-1}) = \frac{1}{2mv(V_2-V_1)}\int_{V_1}^{V_2} I(V)dV \qquad \textbf{Equation 4}$$

$$C_V(F.cm^{-3}) = C_S(F.g^{-1}) * \rho_{electrode} \qquad \textbf{Equation 5}$$

$$E(mWh.cm^{-3}) = \frac{1}{2}C_V(V_2 - V_1)^2 \qquad \textbf{Equation 6}$$

In above equations, C_S is the gravimetric capacitance, v is the potential scan rate, V_1 and V_2 are the low and high end potentials, respectively, I(V) is the response in current, m is the mass loading of the electrode, C_V is the volumetric capacitance, $\rho_{electrode}$ is the density of the electrode (1.67 g·cm^{-3}) and E is the energy density.

The volumetric capacitance values are quite significant in all three different electrolytes studied, highlighting the suitable 2D structure of ERGO-PDA electrodes for charge storage. Only a slight enhancement in capacitance values was observed in the PIL based electrolytes compared to the pristine electrolyte (325 F·cm^{-3} in PIL-water (40/60 wt%) *versus* 311 F·cm^{-3} in 0.5 M Na_2SO_4 (pH=2)) and the rate performance of the composite electrode is quasi-similar in the three electrolytes (**Figure 6a**). The dependence of the capacitance values on the scan rate can be explained by the gradual decrease of pseudo-capacitive contribution from redox reactions with the increase of the scan rate. Furthermore, the repeated CV cycles at a high scan rate (1000 mV·s^{-1}) in 0.5 M Na_2SO_4 (pH=2) and in PIL/water (60/40 wt%) reveal the excellent cycling stability of the ERGO-PDA electrode for 10000 cycles in two electrolytes (**Figure 6b**). The cycling stability of the ERGO-PDA electrode was also evaluated by the continuous galvanostatic charge-discharge (GCD) (**Figure 6c**) and the voltage floating (aging) (**Figure S11**) methods in PIL/water (60/40) + 0.5 M Na_2SO_4. As illustrated in **Figure 6c**, after 10000 continuous cycles at current density of 1 mA·cm^{-2}, 97% of capacitance retention is achieved. **Figure S11** shows the potential-holding curve for 30 h, which shows no significant changes in the GCD curves throughout the aging time, signifying that the ERGO-PDA electrode exhibits excellent stability and no degradation.

We could notice a significant difference when the volumetric energy density of the ERGO-PDA electrode is calculated (**Equation 6**). **Figure 6d** shows that ERGO-PDA has a significantly high volumetric energy density in PIL based electrolytes. In the PIL-water binary mixture, the composite electrode can deliver an energy density of 16.3 $mWhcm^{-3}$ at a scan rate

of 10 mV.s^{-1}, which is almost twice higher than what the same electrode can achieve in the pristine aqueous electrolyte (8.7 $mWh.cm^{-3}$) at the same scan rate. Even at a high cycling rate (1 V·s^{-1}), ERGO-PDA electrode can still deliver an energy density of 6.1 $mWh.cm^{-3}$, which is comparable or higher than most of the recent reports on EDLC electrodes tested in aqueous electrolyte evaluated under similar discharge rates.[27, 47-48] According to the equation used for energy density calculation (**Equation 6**), this significant improvement of the energy density can be explained by the larger potential window in the [Pyr$^+$][HSO$_4^-$]-water binary mixture (60/40 wt%): 1.2 V *versus* only 0.9 V in 0.5 M Na_2SO_4 (pH=2), which is more evidently seen in the CV curves presented in **Figure 1, 3** and **S5**. This behavior is fully in line with the electrogravimetric results which reveal that the water molecules are not implied in the interfacial electrochemical processes when PIL is present in the electrolyte.

4. Conclusions

The processes occurring at the vicinity of the electrode/electrolyte interface are intimately correlated to the electrochemical performance and highly impacted by the choice of the electrolyte composition. Herein, a thorough analysis of interfacial behavior of 2D graphene-polydopamine (ERGO-PDA) composite electrodes was performed in protic ionic liquid [Pyr$^+$][HSO$_4^-$]-water binary mixtures with(out) Na_2SO_4 and compared with the pristine aqueous Na_2SO_4 electrolyte. Due to the high sensitivity of the *ac*-electrogravimetry, we could identify and quantify the charged species and solvent molecules playing a role at the electrode/electrolyte interface, in complex electrolyte compositions involving multiple ions. We could clearly demonstrate that in PIL/water and PIL/water + 0.5 M Na_2SO_4, [Pyr$^+$] cations' contribution to charge compensation is minor compared to H^+ and SO_4^{2-}. Regardless, [Pyr$^+$] has a significant impact in hindering the participation of Na^+ species (when present in the bulk electrolyte) and water molecules (either in the solvation shell or as free H_2O molecules) into the charge compensation process. This behavior is nicely correlated to the electrochemical charge storage performance of the ERGO and ERGO-PDA electrodes. The hindrance of water molecule approach to the interface minimizes the effect of water electrolysis which translates into a larger potential window in the [Pyr$^+$][HSO$_4^-$]-water binary mixture (60/40 wt%) (1.2 V *versus* only 0.9 V in 0.5 M Na_2SO_4 (pH=2)) and thus, a noticeable improvement of the energy density (16.3 $mWh.cm^{-3}$ *versus* 8.7 $mWh.cm^{-3}$ in 0.5 M Na_2SO_4 (pH=2)). Overall, our electrogravimetric study experimentally illustrates the mitigation of the adsorbed water at the electrode/electrolyte interface and how it can improve the electrochemical energy storage

performance, which is exemplified for 2D graphene-polydopamine (ERGO-PDA) composite electrodes.

Associated Content

Supporting Information. Morphological and compositional analyses of ERGO and ERGO-PDA, gravimetric condition verification of QCM – electroacoustic impedance studies, *ac*-electrogravimetry theoretical background, further EQCM and *ac*-electrogravimetry analysis in 0.5 M Na_2SO_4 (pH=2) and in PIL based electrolytes.

Acknowledgements

The authors thank "Doctoral school, "Chimie Physique et Chimie Analytique de Paris-Centre" ED388, French Ministry of Education Scholarship".

Notes

The authors declare no competing financial interest.

Author Information

Corresponding Authors

*E-mail: ozlem.sel@college-de-france.fr

*E-mail: catherine.debiemme-chouvy@sorbonne-universite.fr

References

1. Larcher, D.; Tarascon, J. M., Towards greener and more sustainable batteries for electrical energy storage. *Nat. Chem.* **2015,** *7* (1), 19-29.
2. Liu, L.; Taberna, P.-L.; Dunn, B.; Simon, P., Future Directions for Electrochemical Capacitors. *ACS Energy Lett.* **2021,** *6* (12), 4311-4316.
3. Lv, S.; Ma, L.; Shen, X.; Tong, H., Recent design and control of carbon materials for supercapacitors. *J. Mater. Sci.* **2021,** *56* (3), 1919-1942.
4. Mohd Abdah, M. A. A.; Azman, N. H. N.; Kulandaivalu, S.; Sulaiman, Y., Review of the use of transition-metal-oxide and conducting polymer-based fibres for high-performance supercapacitors. *Mater. Des.* **2020,** *186*, 108199.
5. Zang, X.; Shen, C.; Sanghadasa, M.; Lin, L., High-Voltage Supercapacitors Based on Aqueous Electrolytes. *ChemElectroChem* **2019,** *6* (4), 976-988.
6. Kovalska, E.; Kocabas, C., Organic electrolytes for graphene-based supercapacitor: Liquid, gel or solid. *Mater. Today Commun.* **2016,** *7*, 155-160.

7. Zhang, L.; Yang, S.; Chang, J.; Zhao, D.; Wang, J.; Yang, C.; Cao, B., A Review of Redox Electrolytes for Supercapacitors. *Front Chem* **2020,** *8*, 413-413.
8. Wang, Z.; He, S.; Nguyen, V.; Riley, K. E., Ionic Liquids as Green Solvent and/or Electrolyte for Energy Interface. *Eng. Sci.* **2020,** *11*, 3-18.
9. Watanabe, M.; Thomas, M. L.; Zhang, S.; Ueno, K.; Yasuda, T.; Dokko, K., Application of Ionic Liquids to Energy Storage and Conversion Materials and Devices. *Chem. Rev.* **2017,** *117* (10), 7190-7239.
10. Hui, J.; Gossage, Z. T.; Sarbapalli, D.; Hernández-Burgos, K.; Rodríguez-López, J., Advanced Electrochemical Analysis for Energy Storage Interfaces. *Anal. Chem.* **2019,** *91* (1), 60-83.
11. Yu, X.; Manthiram, A., Electrode–electrolyte interfaces in lithium-based batteries. *Energy Environ. Sci.* **2018,** *11* (3), 527-543.
12. Atkins, D.; Ayerbe, E.; Benayad, A.; Capone, F. G.; Capria, E.; Castelli, I. E.; Cekic-Laskovic, I.; Ciria, R.; Dudy, L.; Edström, K.; Johnson, M. R.; Li, H.; Lastra, J. M. G.; De Souza, M. L.; Meunier, V.; Morcrette, M.; Reichert, H.; Simon, P.; Rueff, J.-P.; Sottmann, J.; Wenzel, W.; Grimaud, A., Understanding Battery Interfaces by Combined Characterization and Simulation Approaches: Challenges and Perspectives. *Adv. Energy Mater.* **2022,** *12* (17), 2102687.
13. Jeong, Y. K.; Park, S. H.; Choi, J. W., Mussel-Inspired Coating and Adhesion for Rechargeable Batteries: A Review. *ACS Appl. Mater. Interfaces* **2018,** *10* (9), 7562-7573.
14. Grey, C. P.; Tarascon, J. M., Sustainability and in situ monitoring in battery development. *Nat. Mater.* **2017,** *16* (1), 45-56.
15. Yang, J.; Muhammad, S.; Jo, M. R.; Kim, H.; Song, K.; Agyeman, D. A.; Kim, Y.-I.; Yoon, W.-S.; Kang, Y.-M., In situ analyses for ion storage materials. *Chem. Soc. Rev.* **2016,** *45* (20), 5717-5770.
16. Levi, M. D.; Salitra, G.; Levy, N.; Aurbach, D.; Maier, J., Application of a quartz-crystal microbalance to measure ionic fluxes in microporous carbons for energy storage. *Nat. Mater.* **2009,** *8* (11), 872-875.
17. Ye, J.; Wu, Y.-C.; Xu, K.; Ni, K.; Shu, N.; Taberna, P.-L.; Zhu, Y.; Simon, P., Charge Storage Mechanisms of Single-Layer Graphene in Ionic Liquid. *J. Am. Chem. Soc.* **2019,** *141* (42), 16559-16563.
18. Lemaire, P.; Dargon, T.; Alves Dalla Corte, D.; Sel, O.; Perrot, H.; Tarascon, J.-M., Making Advanced Electrogravimetry as an Affordable Analytical Tool for Battery Interface Characterization. *Anal. Chem.* **2020,** *92* (20), 13803-13812.
19. Goubaa, H.; Escobar-Teran, F.; Ressam, I.; Gao, W.; El Kadib, A.; Lucas, I. T.; Raihane, M.; Lahcini, M.; Perrot, H.; Sel, O., Dynamic Resolution of Ion Transfer in Electrochemically Reduced Graphene Oxides Revealed by Electrogravimetric Impedance. *J. Phys. Chem. C* **2017,** *121* (17), 9370-9380.
20. Liu, T.; Lin, L.; Bi, X.; Tian, L.; Yang, K.; Liu, J.; Li, M.; Chen, Z.; Lu, J.; Amine, K.; Xu, K.; Pan, F., In situ quantification of interphasial chemistry in Li-ion battery. *Nat. Nanotechnol.* **2019,** *14* (1), 50-56.
21. Dargel, V.; Shpigel, N.; Sigalov, S.; Nayak, P.; Levi, M. D.; Daikhin, L.; Aurbach, D., In situ real-time gravimetric and viscoelastic probing of surface films formation on lithium batteries electrodes. *Nat. Commun.* **2017,** *8* (1), 1389.
22. Griffin, J. M.; Forse, A. C.; Tsai, W.-Y.; Taberna, P.-L.; Simon, P.; Grey, C. P., In situ NMR and electrochemical quartz crystal microbalance techniques reveal the structure of the electrical double layer in supercapacitors. *Nat. Mater.* **2015,** *14* (8), 812-819.
23. Kwon, K.; Kong, F.; McLarnon, F.; Evans, J. W., Characterization of the SEI on a Carbon Film Electrode by Combined EQCM and Spectroscopic Ellipsometry. *J. Electrochem. Soc.* **2003,** *150* (2), A229.

24. Tsai, W.-Y.; Taberna, P.-L.; Simon, P., Electrochemical Quartz Crystal Microbalance (EQCM) Study of Ion Dynamics in Nanoporous Carbons. *J. Am. Chem. Soc.* **2014,** *136* (24), 8722-8728.
25. Gabrielli, C.; García-Jareño, J. J.; Keddam, M.; Perrot, H.; Vicente, F., Ac-Electrogravimetry Study of Electroactive Thin Films. I. Application to Prussian Blue. *J. Phys. Chem B* **2002,** *106* (12), 3182-3191.
26. Arias, C. R.; Debiemme-Chouvy, C.; Gabrielli, C.; Laberty-Robert, C.; Pailleret, A.; Perrot, H.; Sel, O., New Insights into Pseudocapacitive Charge-Storage Mechanisms in Li-Birnessite Type MnO2 Monitored by Fast Quartz Crystal Microbalance Methods. *J. Phys. Chem. C* **2014,** *118* (46), 26551-26559.
27. Bouzina, A.; Perrot, H.; Sel, O.; Debiemme-Chouvy, C., Preventing Graphene from Restacking via Bioinspired Chemical Inserts: Toward a Superior 2D Micro-supercapacitor Electrode. *ACS Appl. Nano Mater.* **2021,** *4* (5), 4964-4973.
28. Burrell, G. L.; Burgar, I. M.; Separovic, F.; Dunlop, N. F., Preparation of protic ionic liquids with minimal water content and 15N NMR study of proton transfer. *Phys. Chem. Chem. Phys.* **2010,** *12* (7), 1571-1577.
29. Brandt, A.; Pires, J.; Anouti, M.; Balducci, A., An investigation about the cycling stability of supercapacitors containing protic ionic liquids as electrolyte components. Electrochim. Acta **2013,** *108*, 226-231.
30. Timperman, L.; Galiano, H.; Lemordant, D.; Anouti, M., Phosphonium-based protic ionic liquid as electrolyte for carbon-based supercapacitors. *Electrochem. commun.* **2011,** *13* (10), 1112-1115.
31. Al-Zohbi, F.; Jacquemin, J.; Ghamouss, F.; Schmaltz, B.; Abarbri, M.; Cherry, K.; Tabcheh, M. F.; Tran-Van, F., Impact of the aqueous pyrrolidinium hydrogen sulfate electrolyte formulation on transport properties and electrochemical performances for polyaniline-based supercapacitor. *J. Power Sources* **2019,** *431*, 162-169.
32. Anouti, M.; Caillon-Caravanier, M.; Dridi, Y.; Galiano, H.; Lemordant, D., Synthesis and Characterization of New Pyrrolidinium Based Protic Ionic Liquids. Good and Superionic Liquids. *J. Phys. Chem B* **2008,** *112* (42), 13335-13343.
33. Anouti, M.; Porion, P.; Brigouleix, C.; Galiano, H.; Lemordant, D., Transport properties in two pyrrolidinium-based protic ionic liquids as determined by conductivity, viscosity and NMR self-diffusion measurements. *Fluid Ph. Equilibria* **2010,** *299* (2), 229-237.
34. Sauerbrey, G., Verwendung von Schwingquarzen zur Wägung dünner Schichten und zur Mikrowägung. Z. Phys. **1959,** *155*, 206-222.
35. Bizet, K.; Gabrielli, C.; Perrot, H., Immunodetection by quartz crystal microbalance. A new approach for direct detection of rabbit IgG and peroxidase. *Appl. Biochem. Biotechnol.* **2000,** *89* (2-3), 139-49.
36. Alassi, A.; Benammar, M.; Brett, D., Quartz Crystal Microbalance Electronic Interfacing Systems: A Review. *Sensors (Basel, Switzerland)* **2017,** *17* (12).
37. Gao, W.; Debiemme-Chouvy, C.; Lahcini, M.; Perrot, H.; Sel, O., Tuning Charge Storage Properties of Supercapacitive Electrodes Evidenced by In Situ Gravimetric and Viscoelastic Explorations. *Anal. Chem.* **2019,** *91* (4), 2885-2893.
38. Gao, W.; Demir-Cakan, R.; Perrot, H.; Sel, O., Electrochemically Reduced Graphene Oxide-Sheltered ZnO Nanostructures Showing Enhanced Electrochemical Performance Revealed by an In Situ Electrogravimetric Study. *Adv. Mater. Interfaces* **2019,** *6* (5), 1801855.
39. Plausinaitis, D.; Ratautaite, V.; Mikoliunaite, L.; Sinkevicius, L.; Ramanaviciene, A.; Ramanavicius, A., Quartz Crystal Microbalance-Based Evaluation of the Electrochemical Formation of an Aggregated Polypyrrole Particle-Based Layer. *Langmuir* **2015,** *31* (10), 3186-3193.

40. Agrisuelas, J.; Gabrielli, C.; García-Jareño, J. J.; Perrot, H.; Sel, O.; Vicente, F., Viscoelastic potential-induced changes in acoustically thin films explored by quartz crystal microbalance with motional resistance monitoring. *Electrochim. Acta* **2015,** *176*, 1454-1463.
41. Mysyk, R.; Raymundo-Piñero, E.; Anouti, M.; Lemordant, D.; Béguin, F., Pseudo-capacitance of nanoporous carbons in pyrrolidinium-based protic ionic liquids. *Electrochem. commun.* **2010,** *12* (3), 414-417.
42. Hurt, R., Chemistry and Physics of Carbon. Volume 27 Edited by Ljubisa R. Radovic (Pennsylvania State University). Marcel Dekker: New York, Basel. 2001. *J. Am. Chem. Soc.* **2001,** *123* (41), 10141-10141.
43. Montes-Morán, M. A.; Suárez, D.; Menéndez, J. A.; Fuente, E., On the nature of basic sites on carbon surfaces: an overview. *Carbon* **2004,** *42* (7), 1219-1225.
44. Jurewicz, K.; Frackowiak, E.; Béguin, F., Towards the mechanism of electrochemical hydrogen storage in nanostructured carbon materials. *Appl. Phys.* **A 2004,** *78* (7), 981-987.
45. Levi, M. D.; Sigalov, S.; Salitra, G.; Elazari, R.; Aurbach, D., Assessing the Solvation Numbers of Electrolytic Ions Confined in Carbon Nanopores under Dynamic Charging Conditions. *J. Phys. Chem. Lett.* **2011,** *2* (2), 120-4.
46. Shpigel, N.; Levi, M. D.; Sigalov, S.; Mathis, T. S.; Gogotsi, Y.; Aurbach, D., Direct Assessment of Nanoconfined Water in 2D Ti_3C_2 Electrode Interspaces by a Surface Acoustic Technique. *J. Am. Chem. Soc.* **2018,** *140* (28), 8910-8917.
47. Li, G.; Mao, K.; Liu, M.; Yan, M.; Zhao, J.; Zeng, Y.; Yang, L.; Wu, Q.; Wang, X.; Hu, Z., Achieving Ultrahigh Volumetric Energy Storage by Compressing Nitrogen and Sulfur Dual-Doped Carbon Nanocages via Capillarity. *Adv. Mater.* **2020,** *32* (52), 2004632.
48. Tao, Y.; Xie, X.; Lv, W.; Tang, D.-M.; Kong, D.; Huang, Z.; Nishihara, H.; Ishii, T.; Li, B.; Golberg, D.; Kang, F.; Kyotani, T.; Yang, Q.-H., Towards ultrahigh volumetric capacitance: graphene derived highly dense but porous carbons for supercapacitors. *Sci. Rep.* **2013,** *3* (1), 2975.

TOC Graphics

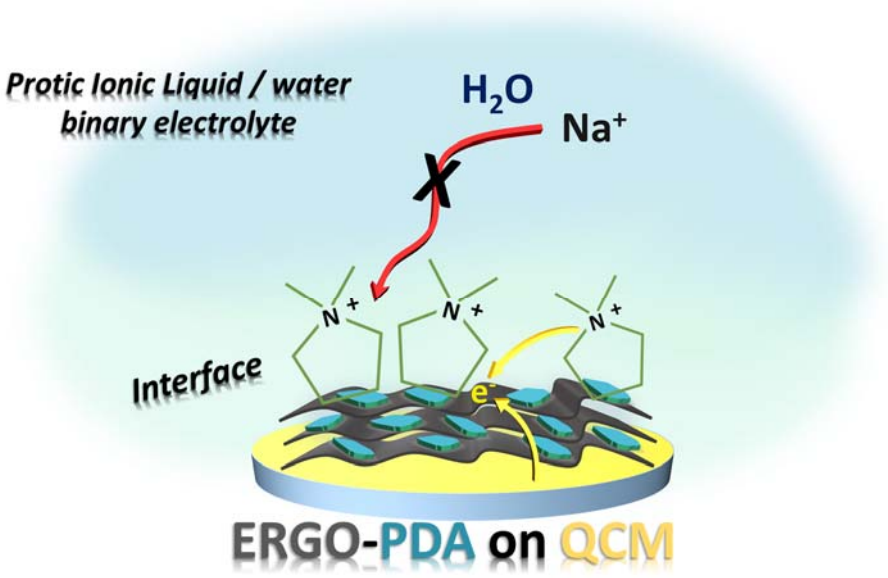

Supporting Information

Interface properties of 2D graphene-polydopamine composite electrodes in protic ionic liquid based electrolytes explored by advanced electrogravimetry

Adnane Bouzina,[a] Hubert Perrot,[a] Catherine Debiemme-Chouvy[a,*] and Ozlem Sel[b,c,*]

[a] Sorbonne Université, CNRS, Laboratoire Interfaces et Systèmes Electrochimiques, LISE, UMR 8235, 4 Place Jussieu, 75005 Paris, France

[b] Chimie du Solide et de l'Energie, UMR 8260, Collège de France, 11 Place Marcelin Berthelot, 75231 Paris Cedex 05, France

[c] Réseau sur le Stockage Electrochimique de l'Energie (RS2E), CNRS FR 3459, 33 Rue Saint Leu, 80039 Amiens Cedex, France

Corresponding Authors

*E-mail: ozlem.sel@college-de-france.fr

*E-mail: catherine.debiemme-chouvy@sorbonne-universite.fr

Table of contents

Part I. Morphological and Compositional analysis	S2
Part II. Gravimetric condition verification of QCM – electroacoustic impedance studies	S2
Part III. *Ac*-electrogravimetry theoretical background	S3
Part IV. Gravimetric EQCM and *ac*-electrogravimetry analysis in 0.5 M Na_2SO_4 (pH=2)	S6
Part V. Gravimetric EQCM and *ac*-electrogravimetry analysis in PIL based electrolytes	S8
Part VI. Stability tests of the electrodes	S12
References	S12

Part I. Morphological and Compositional analysis

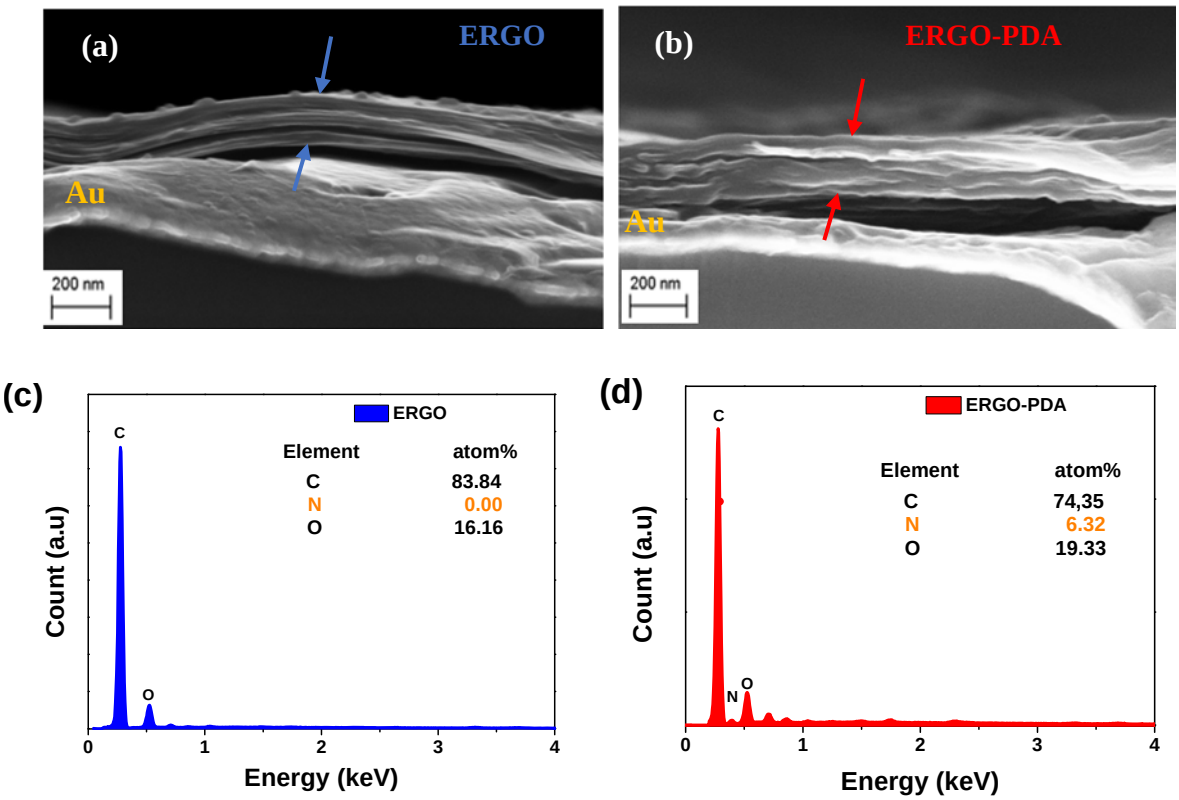

Figure S1. FEG-SEM micrographs of the cross-section of (a) ERGO and (b) ERGO-PDA. EDX analysis of (c) ERGO and (d) ERGO-PDA.

Part II. Gravimetric condition verification of QCM – electroacoustic impedance studies

Table S1. The resonant frequency and the motional resistance of the blank quartz. ERGO and ERGO-PDA electrodes at different states.

	Resonant frequency (Hz)	Motional resistance (R_1) (Ω)
Blank quartz in air	9 000 535	6
Blank quartz in Na_2SO_4 (pH=2)	8 997 578	395
ERGO in air	8 994 020	7
ERGO-PDA in air	8 994 943	8
ERGO in Na_2SO_4 (pH=2)	8 989 272	449
ERGO-PDA in Na_2SO_4 (pH=2)	8 988 830	486

In the order to verify the gravimetric regime of our films in air and the electrolyte, the registered motional resistance was converted to total resonance width, ΔW (where $\Delta W/2 = \Delta\Gamma$ is the half-width at half-height of the resonance peak). Contrary to the motional resistance, the ΔW has the

same dimension as the frequency (Hz) and can therefore be linked to the variation of the resonant frequency. The condition for gravimetric regime is described as $|\Delta W| \ll |\Delta f/n|$, with n is the overtone which equals to 1 in the present case. The following equation can be used to determine the coefficient joining R_1 and W:[1-2]

$$W = \frac{32 A e_{26}{}^2 \rho_q{}^2 f_0{}^3}{\pi \sqrt{\mu_q \rho_q}^3} R_1 \qquad \textbf{Eq. S1}$$

where A is the piezoelectrically active area (0.2 10^{-4} $A \cdot m^2$), e_{26} is the piezoelectric stress coefficient (9.65 10^{-2} $A \cdot s \cdot m^{-2}$ for AT-cut quartz), ρ_q is the density of the quartz (2.648 10^3 $kg \cdot m^{-3}$), f_0 is the resonant frequency (9 000 520 Hz), and μ_q is the shear modulus (2.947 10^{10} $kg \cdot m^{-1} \cdot s^{-2}$).

The value of 13.82 $Hz \cdot \Omega^{-1}$ was found for the W/R_1 ratio and used to obtain **Table S2**, which compares the bare and loaded quartz resonators in air and in electrolyte. The ratios $|\Delta W|/|\Delta f|$ of the ERGO and ERGO-PDA electrodes measured in air and in 0.5 M Na_2SO_4 (pH=2) are presented in **Table S2**. A ratio $|\Delta W|/|\Delta f| << 1$ ensures the gravimetric regime of the coating.

Table S2: $|\Delta W|/|\Delta f|$ of the ERGO and ERGO-PDA electrodes measured in air and in 0.5 M Na_2SO_4 (pH=2).

	$|\Delta W|/|\Delta f|$ calculated during the film generation	
Electrode coating	**Air**	**Na_2SO_4 (pH=2)**
ERGO	**0.0001**	**0.09**
ERGO-PDA	**0.0036**	**0.12**

Part III. *Ac*-electrogravimetry theoretical background

The *ac*-electrogravimetry methodology and theoretical background were previously discussed by Gabrielli *et al.*[3-4] Briefly, *ac*-electrogravimetry consists of coupling electrochemical impedance spectroscopy (EIS) with a fast quartz crystal microbalance (QCM) used in *ac*-mode. It allows the mass change, Δm, of the working electrode to be measured simultaneously with the AC response, ΔI, of the electrochemical system. This leads to $\frac{\Delta E}{\Delta I}(\omega)$, electrical transfer function, $\frac{\Delta q}{\Delta E}(\omega)$, the charge/potential transfer function and $\frac{\Delta m}{\Delta I}(\omega)$, mass-potential transfer

function to be simultaneously obtained owing to a sinusoidal potential perturbation with a small amplitude. The combination of such transfer functions provides the possibility of a fair separation of different electrochemical processes, which involves concomitantly the charge and mass changes.

The various transfer functions, mainly $\frac{\Delta E}{\Delta I}(\omega)$, $\frac{\Delta q}{\Delta E}(\omega)$ and $\frac{\Delta m}{\Delta I}(\omega)$ can be theoretically calculated through the following **Equations S2** to **S5**:

$$\frac{\Delta C_i}{\Delta E}(\omega)\Big|_{th} = \frac{-G_i}{j\omega d_f + K_i}(\omega) \qquad \textbf{Eq. S2}$$

$$\frac{\Delta q}{\Delta E}(\omega)\Big|_{th} = \quad \text{(i: charged species)} \qquad \textbf{Eq. S3}$$

$$\frac{\Delta q}{\Delta E}(\omega)\Big|_{th} = F d_f \sum_i \frac{G_i}{j\omega d_f + K_i}(\omega) \quad \text{(i: charged species)} \qquad \textbf{Eq. S4}$$

$$\frac{\Delta m}{\Delta E}(\omega)\Big|_{th} = -d_f \sum_i M_i \frac{G_i}{j\omega d_f + K_i}(\omega) \quad \text{(i: (non)charged species)} \qquad \textbf{Eq. S5}$$

where ΔC_i presents the concentration variation for each species (ions and free solvent) in electrodes, ω the pulsation, d_f the film thickness (estimated through QCM measurements and the density of the material), M_i the atomic weight of involved species, K_i and G_i are the partial derivatives of the flux (J_i) with respect to the concentration of the species, *i* and the potential, respectively. K_i represents the kinetics of transfer of each species whereas G_i describes the level of difficulty for each species transferred at the electrode/electrolyte interface.

To illustrate what the experimental *ac*-electrogravimetry data may look like, the $\frac{\Delta E}{\Delta I}(\omega)$, $\frac{\Delta q}{\Delta E}(\omega)$ and $\frac{\Delta m}{\Delta I}(\omega)$ transfer functions (TFs) are shown schematically in **Scheme S1a-f**. For a single ion transfer at the electrode/electrolyte interface, a typical cation and anion contribution appear characteristically on the third and the first quadrant (Cartesian system) of the $\frac{\Delta m}{\Delta I}(\omega)$ (**Scheme S1c**, **f**), respectively.

It is important to note that the $\frac{\Delta m}{\Delta I}(\omega)$ is the only TF that can discriminate between the cations or anions and identify them by their molar mass (M_i in **Equation S5**). In a more complex electrochemical process, where a multi-ion transfer occurs, the above mentioned TFs may look like as shown in **Scheme S1d-f**. The low frequency response of the $\frac{\Delta E}{\Delta I}(\omega)$ (**Scheme S1d**) may translate into two separate loops in $\frac{\Delta q}{\Delta E}(\omega)$ (**Scheme S1e**), if the respective time constants of the participating ions are different enough. However, it is noted that the four different configurations given in **Scheme S1e** result in the same response in terms of $\frac{\Delta q}{\Delta E}(\omega)$ TF. The utility

and the power of the $\frac{\Delta m}{\Delta I}(\omega)$ TF is more evident in **Scheme S1f**, where 4 possibilities of ionic transfers (two cations, two anions, a cation/anion and an anion/cation) can be distinguished, with further kinetic resolution depending on the dynamics of interfacial transfer.

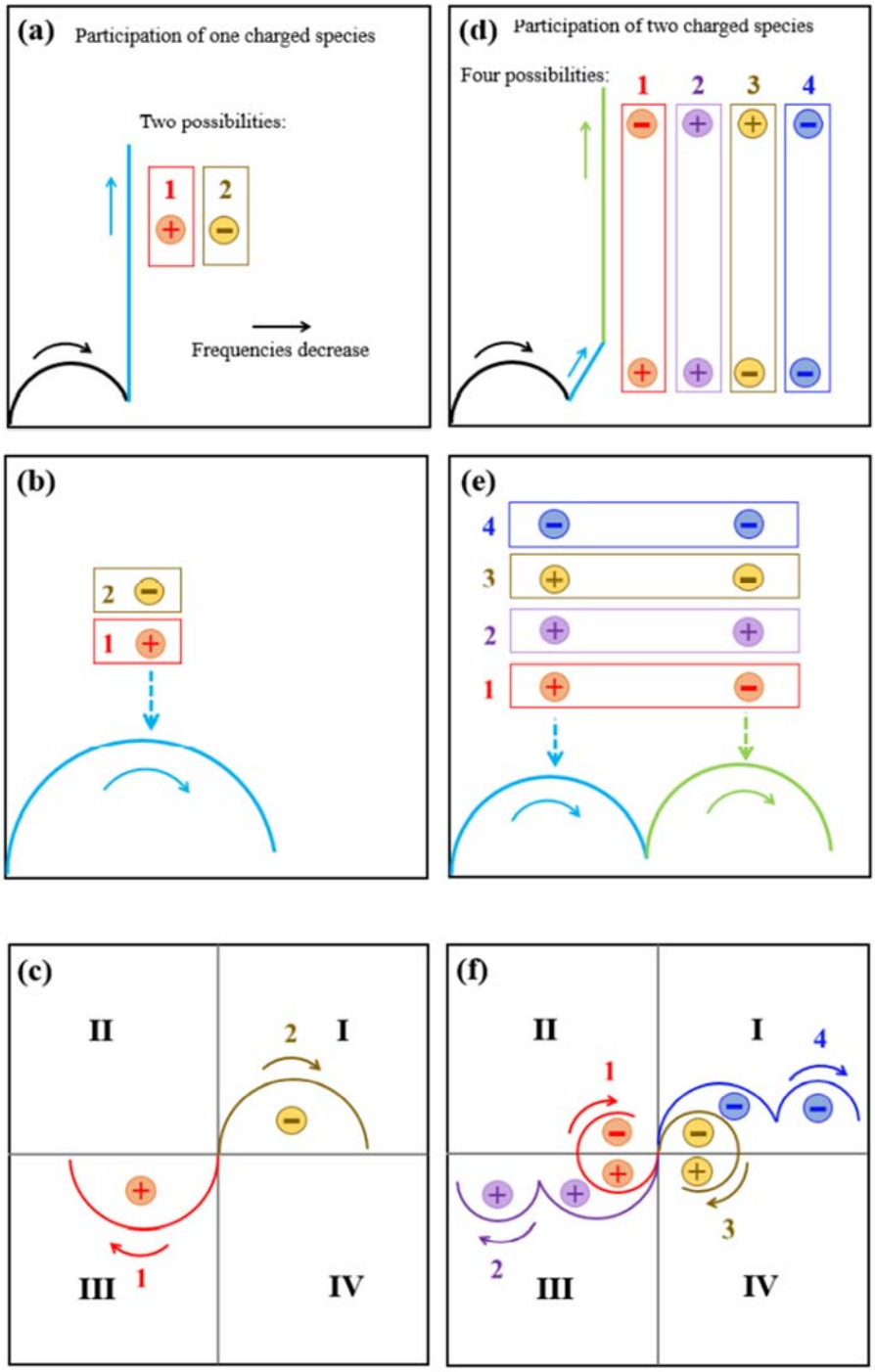

Scheme S1. Representation different simulated Transfer Functions (TFs) for $\Delta E/\Delta I(\omega)$ (a, d). $\Delta q/\Delta E(\omega)$ (b, e) and $\Delta m/\Delta E(\omega)$ (c, f). The response of one and two charged species is depicted in (a, b, c) and (d, e, f), respectively. Note: H_2O contribution is not taken into account, which

can participate in charge compensation either in the free form with the same direction of a cation/anion flux or in the hydration shell of cation/anion. In these representations, the time constants of ionic species are different enough so that they are seen as separate contributions.[5]

Part IV. Gravimetric EQCM and *ac*-electrogravimetry analysis in 0.5 M Na_2SO_4 (pH=2)

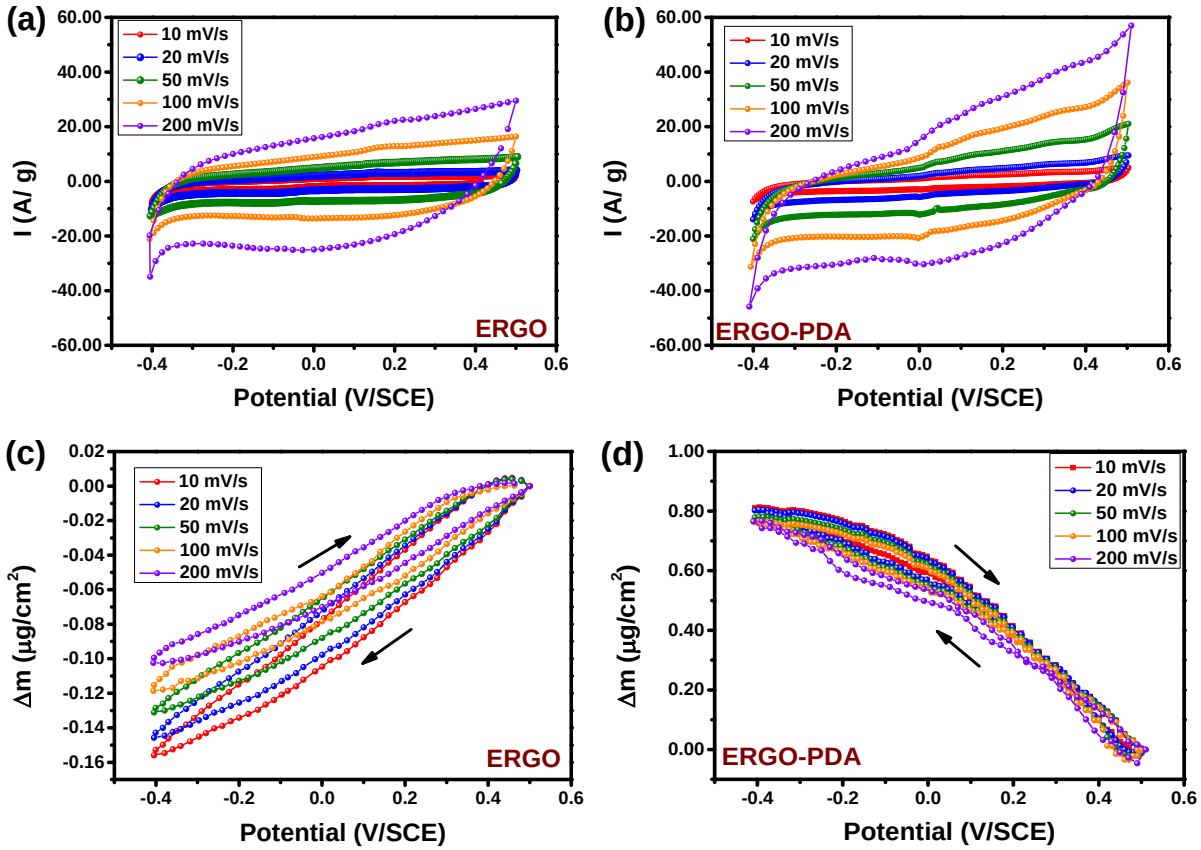

Figure S2. (a-b) CV and (c-d) mass change *vs* applied potential of ERGO and ERGO-PDA at different potential scan rates in 0.5 M Na_2SO_4 (pH=2).

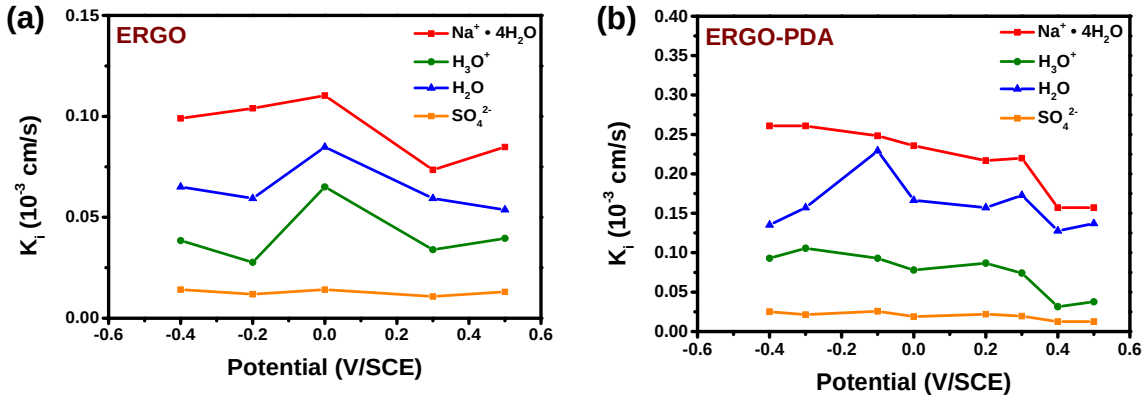

Figure S3. Kinetic constants of interfacial transfer. K_i. ERGO (a). ERGO-PDA (b) estimated from the fitting of the *ac*-electrogravimetric data and measured in 0.5 M Na_2SO_4 (pH=2).

Table S3. G_i /K_i values obtained from the fitting of the *ac*-electrogravimetric data measured in 0.5 M Na_2SO_4 (pH=2) at different potentials for ERGO electrode.

Potential (V/SCE)	G_{C1}/K_{C1} (*10^4)	G_{C2}/K_{C2} (*10^4)	G_{H2O}/K_{H2O} (*10^4)	$G_{SO4^{2-}}/K_{SO4^{2-}}$ (*10^4)	% G_{C1}/K_{C1}	% G_{C2}/K_{C2}	% G_{H2O}/K_{H2O}	% $G_{SO4^{2-}}/K_{SO4^{2-}}$
0.5	**2**	**3**	**3**	**-10**	**11**	**17**	**17**	**55**
0.3	**2**	**6**	**7**	**-8**	**9**	**26**	**30**	**35**
0	**1**	**6**	**3**	**-9**	**5**	**32**	**16**	**47**
-0.2	**1**	**6**	**12**	**-7**	**4**	**23**	**46**	**27**
-0.4	**1**	**5**	**11**	**-9**	**4**	**19**	**42**	**35**

Table S4. G_i/K_i values obtained from the fitting of the *ac*-electrogravimetric data measured in 0.5 M Na_2SO_4 (pH=2) at different potentials for ERGO-PDA electrode.

Potential (V/SCE)	G_{C1}/K_{C1} (*10^4)	G_{C2}/K_{C2} (*10^4)	G_{H2O}/K_{H2O} (*10^4)	$G_{SO4^{2-}}/K_{SO4^{2-}}$ (*10^4)	% G_{C1}/K_{C1}	% G_{C2}/K_{C2}	% G_{H2O}/K_{H2O}	% $G_{SO4^{2-}}/K_{SO4^{2-}}$
0.5	**7**	**11**	**11**	**-11**	**18**	**27**	**28**	**27**
0.4	**6**	**11**	**6**	**-7**	**20**	**37**	**20**	**23**
0.3	**4**	**6**	**9**	**-6**	**16**	**25**	**36**	**24**
0.2	**3**	**10**	**17**	**-7**	**8**	**27**	**46**	**19**
0	**2**	**8**	**5**	**-6**	**9**	**38**	**24**	**29**
-0.1	**2**	**8**	**18**	**-8**	**6**	**22**	**50**	**22**
-0.3	**2**	**8**	**23**	**-8**	**5**	**20**	**56**	**18**
-0.4	**2**	**7**	**28**	**-9**	**4**	**16**	**61**	**19**

Part V. Gravimetric EQCM and *ac*-electrogravimetry analysis in PIL/water based electrolytes

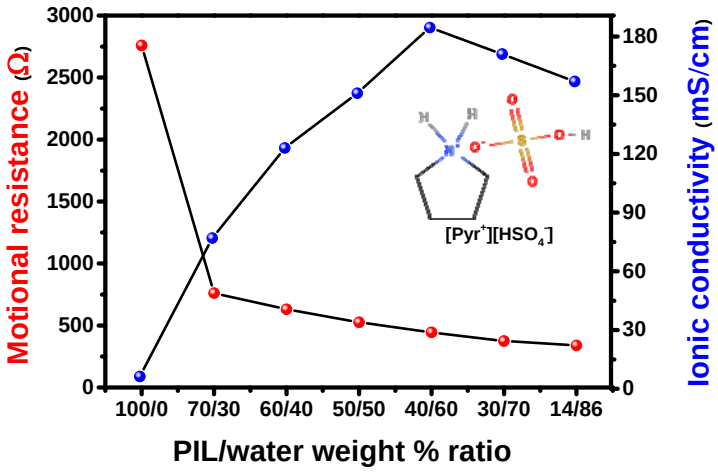

Figure S4. Evolution of the motional resistance of blank quartz and the ionic conductivity of the $[Pyr^+][HSO_4^-]$ as a function of water content expressed in PIL/water weight % ratio.

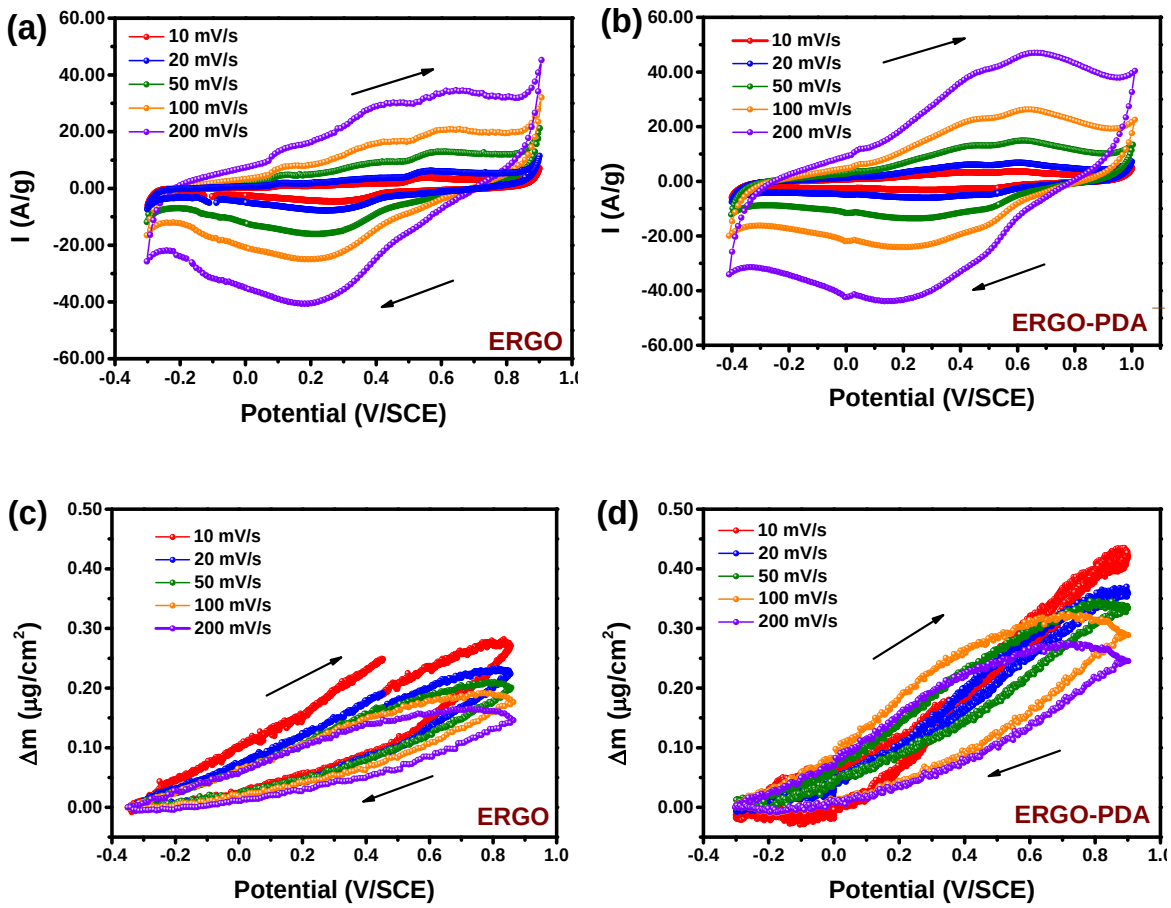

Figure S5. (a-b) CV and (c-d) mass change *vs*. applied potential of ERGO and ERGO-PDA at different potential scan rates in PIL/water (40/60 wt%) + 0.5 M Na_2SO_4.

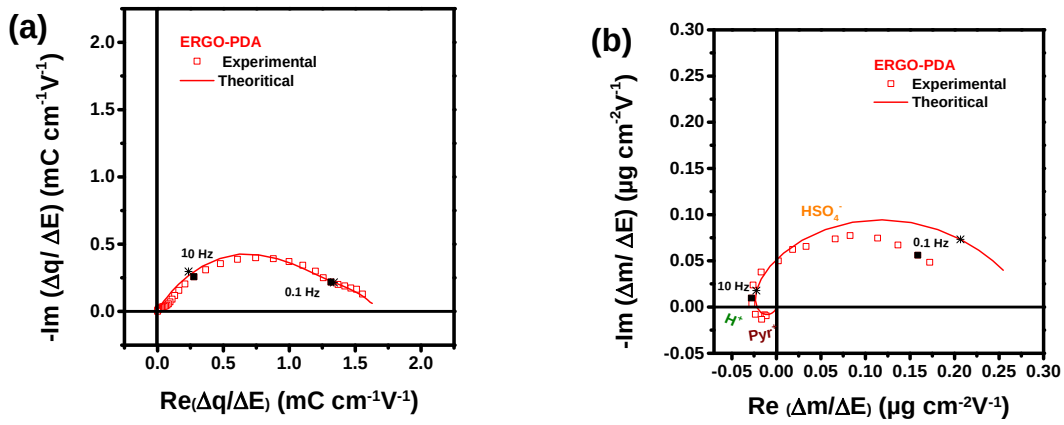

Figure S6. Experimental and theoretical curves for *ac*-electrogravimetry analyses of ERGO-PDA at 0 V *vs* SCE. (a) $\Delta q/\Delta E(\omega)$, (b) $\Delta m/\Delta E(\omega)$ in $[Pyr^+][HSO_4^-]$-water binary mixture (60/40 wt%) in presence of 0.5 M Na_2SO_4.

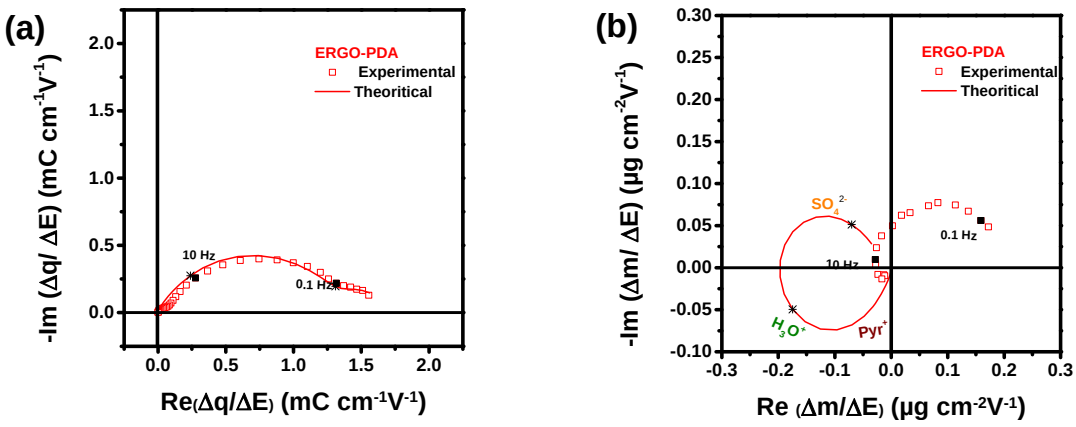

Figure S7. Experimental and theoretical *ac*-electrogravimetric data of ERGO-PDA at 0 V *vs* SCE. (a) $\Delta q/\Delta E(\omega)$, (b) $\Delta m/\Delta E(\omega)$ in $[Pyr^+][HSO_4^-]$-water binary mixture (60/40 wt%) in presence of 0.5 M Na_2SO_4.

Charge fraction calculation of each ion, estimated from ac-electrogravimetry

$$\%\,c1 = \frac{\dfrac{Gc1}{Kc1}}{\dfrac{Gc1}{Kc1} + \dfrac{Gc2}{Kc2} + \dfrac{Gs}{Ks} + \dfrac{|Ga|}{Ka}} \qquad \textbf{Eq. S6}$$

$$\%c2 = \frac{\frac{Gc2}{Kc2}}{\frac{Gc1}{Kc1} + \frac{Gc2}{Kc2} + \frac{Gs}{Ks} + \frac{|Ga|}{Ka}}$$ **Eq. S7**

$$\%s = \frac{\frac{Gs}{Ks}}{\frac{Gc1}{Kc1} + \frac{Gc2}{Kc2} + \frac{Gs}{Ks} + \frac{|Ga|}{Ka}}$$ **Eq. S8**

$$\%a = \frac{\frac{|Ga|}{Ka}}{\frac{Gc1}{Kc1} + \frac{Gc2}{Kc2} + \frac{Gs}{Ks} + \frac{|Ga|}{Ka}}$$ **Eq. S9**

$$\Delta m_{ac-QCM} = (Q - Q_0) \times (\%c1 \times M_{c1} + \%c2 \times M_{c2} + \%s \times M_s + \%a \times M_a) / F$$

Eq. S10

$$\Delta m_i = \%i \times (Q - Q_0) \times (M_i) / F$$ **Eq. S11**

where (Q-Q_0) is the charge (it is calculated from to anodic sweep of potential of the CV responses at 10 mV s^{-1}) and F is the Faraday constant (96485 C/mol).

In the case of the baseline electrolyte Na_2SO_4 (pH = 2), M_{c1}, M_{c2}, M_s and M_a are the molar masses of $Na^+.4H_2O$, H_3O^+, H_2O and SO_4^{2-}, respectively.

In the case of PIL-based electrolytes M_{c1}, M_{c2} and M_a are the molar masses of Pyr^+, H^+ and SO_4^{2-}, respectively.

The **Eq. S11** involves, Δm_i, which represents the contribution of the species, i, to the global mass response.

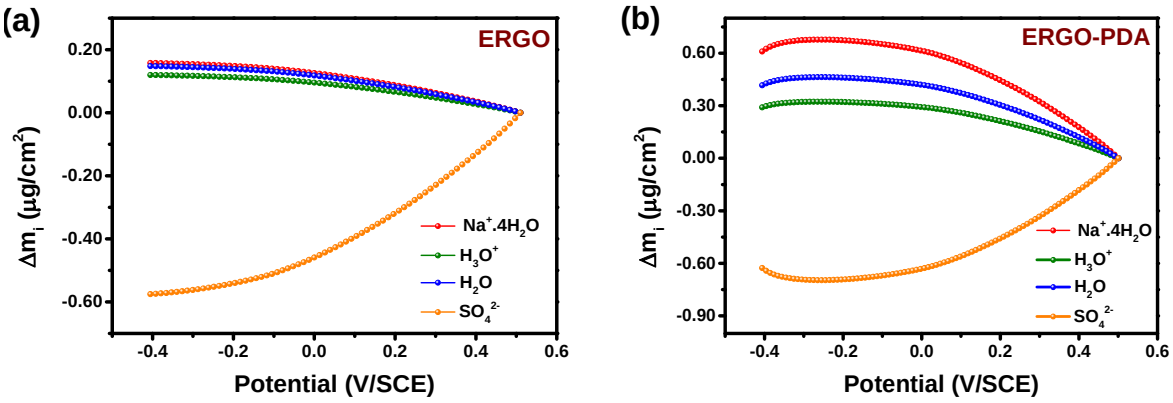

Figure S8. The theoretical mass variation of the (a) ERGO and (b) ERGO-PDA electrodes, separating the global mass variation into several species contribution (calculated using **Eq. S11**) in Na_2SO_4 (pH = 2).

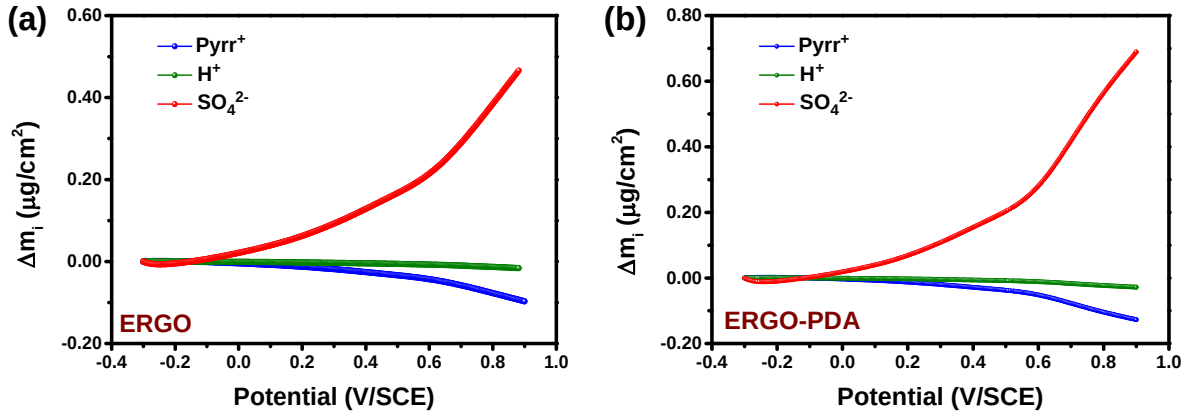

Figure S9. The theoretical mass variation of the (a) ERGO and (b) ERGO-PDA electrodes, separating the global mass variation into several species contribution (calculated using **Eq.S11**) in PIL/water (40/60 wt%).

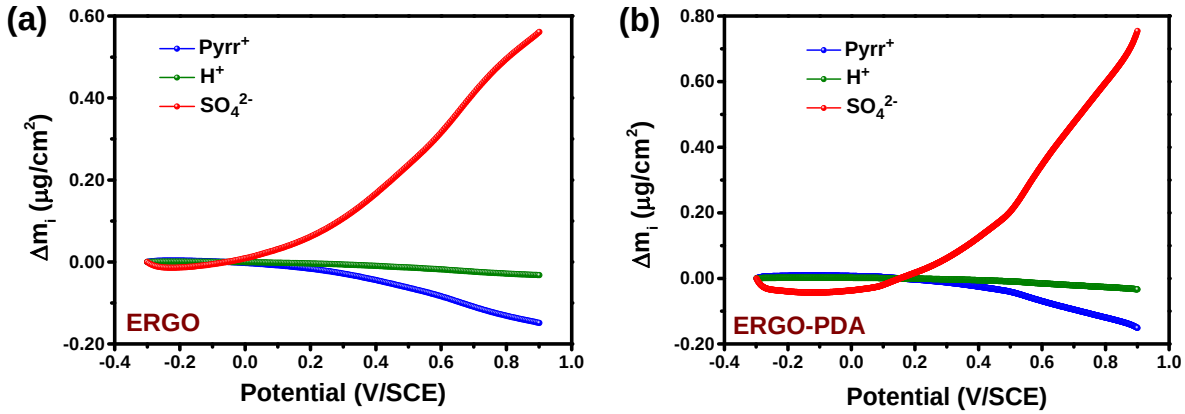

Figure S10. The theoretical mass variation of the (a) ERGO and (b) ERGO-PDA electrodes, separating the global mass variation into several species contribution (calculated using **Eq. S11**) in PIL/water (40/60 wt%) + 0.5 M Na_2SO_4.

Part VI. Stability test of the electrodes

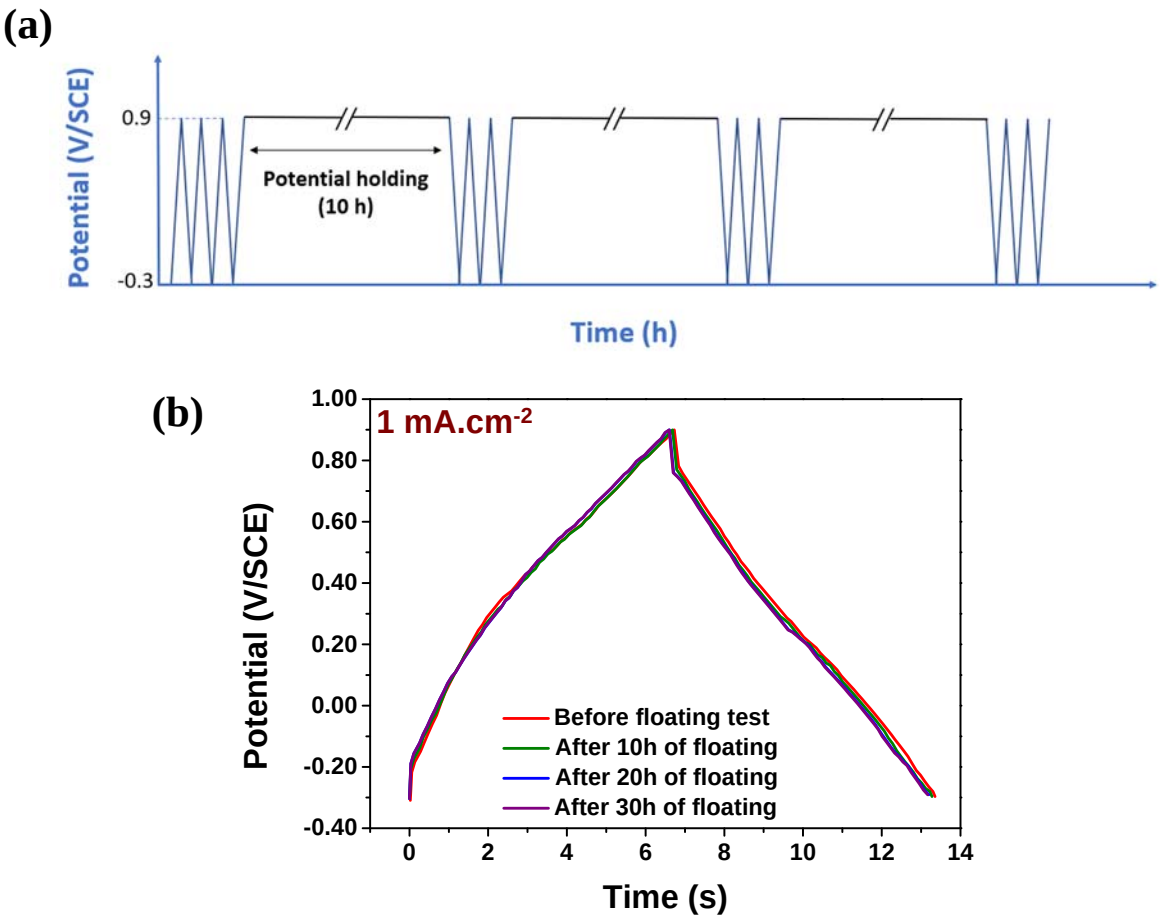

Figure S11. (a) Schematic illustration of the floating test experiment at 0.9V/SCE and (b) the charge-discharge curve at a current density of 1 mA.cm^{-2}, measured after a potential floating period of ERGO-PDA in PIL/water (60/40 wt%) + 0.5 M Na_2SO_4.

References

1. Lemaire. P.; Dargon. T.; Alves Dalla Corte. D.; Sel. O.; Perrot. H.; Tarascon. J.-M. Making Advanced Electrogravimetry as an Affordable Analytical Tool for Battery Interface Characterization. *Analytical Chemistry* **2020**, *92* (20), 13803-13812.
2. Johannsmann. D.. The Quartz Crystal Microbial in Soft Matter Research: Fundamentals and Modeling. *Springers International Publishing* **2015**.
3. Gabrielli. C.; García-Jareño. J. J.; Keddam. M.; Perrot. H.; Vicente. F. Ac-Electrogravimetry Study of Electroactive Thin Films. I. Application to Prussian Blue. *The Journal of Physical Chemistry B* **2002**, *106* (12), 3182-3191.
4. Gabrielli. C.; Garcia-Jareño. J. J.; Keddam. M.; Perrot. H.; Vicente. F. Ac-Electrogravimetry Study of Electroactive Thin Films. II. Application to Polypyrrole. *The Journal of Physical Chemistry B* **2002**, *106* (12), 3192-3201.
5. Gao. W.; Debiemme-Chouvy. C.; Lahcini. M.; Perrot. H.; Sel. O. Tuning Charge Storage Properties of Supercapacitive Electrodes Evidenced by In Situ Gravimetric and Viscoelastic Explorations. *Analytical Chemistry* **2019**, *91* (4), 2885-2893.